Geostatistical analysis of an experimental stratigraphy

Ye Zhang,[1,2] Mark Person,[1] Chris Paola,[3] Carl W. Gable,[4] Xian-Huan Wen,[5] and J. Matthew Davis[6]

Received 21 October 2004; revised 13 May 2005; accepted 1 July 2005; published 16 November 2005.

[1] A high-resolution stratigraphic image of a flume-generated deposit was scaled up to sedimentary basin dimensions where a natural log hydraulic conductivity (ln(K)) was assigned to each pixel on the basis of gray scale and conductivity end-members. The synthetic ln(K) map has mean, variance, and frequency distributions that are comparable to a natural alluvial fan deposit. A geostatistical analysis was conducted on selected regions of this map containing fluvial, fluvial/floodplain, shoreline, turbidite, and deepwater sedimentary facies. Experimental ln(K) variograms were computed along the major and minor statistical axes and horizontal and vertical coordinate axes. Exponential and power law variogram models were fit to obtain an integral scale and Hausdorff measure, respectively. We conclude that the shape of the experimental variogram depends on the problem size in relation to the size of the local-scale heterogeneity. At a given problem scale, multilevel correlation structure is a result of constructing variogram with data pairs of mixed facies types. In multiscale sedimentary systems, stationary correlation structure may occur at separate scales, each corresponding to a particular hierarchy; the integral scale fitted thus becomes dependent on the problem size. The Hausdorff measure obtained has a range comparable to natural geological deposits. It increases from nonstratified to stratified deposits with an approximate cutoff of 0.15. It also increases as the number of facies incorporated in a problem increases. This implies that fractal characteristic of sedimentary rocks is both depositional process–dependent and problem-scale-dependent.

Citation: Zhang, Y., M. Person, C. Paola, C. W. Gable, X.-H. Wen, and J. M. Davis (2005), Geostatistical analysis of an experimental stratigraphy, *Water Resour. Res.*, *41*, W11416, doi:10.1029/2004WR003756.

1. Introduction

[2] The correlation range estimated for natural log hydraulic conductivity (ln(K)) in sedimentary deposits has been found to increase as the observation scale increases [*Gelhar*, 1993]. Different interpretations have been offered for the apparent growth in ln(K) correlation range. *Gelhar* [1993] proposed a multilevel, nested model for lag separations ranging from core scale (10^{-1} m), fluvial deposit scale (10^{1} m), alluvial basin scale (10^{3} m), up to interbasin scale (10^{5} m). The nested model contains multiple sills in a well-defined hierarchical structure with increasing levels of ln(K) variability corresponding to distinct ranges of lag separation. On the other hand, the "scale effect" observed in solute dispersion is linked to the growth of ln(K) correlation for which a power law variogram model was proposed [*Neuman*, 1990, 1994]. Under this hypothesis, the ln(K) random field is self-affine and constitutes a particular class of stochastic fractal called fractional Brownian motion (fBm). The spectral density of a fBm has a power law dependence on the wave number with a power law exponent (spectral slope) ranging from 1 to 3 [*Turcotte*, 1997]. Different stochastic fractals have also been proposed to characterize ln(K) variability (e.g., fractional Gaussian noise or fGn; fractional Levy motion or fLm and fractional Levy noise or fLn for non-Gaussian processes) [*Molz and Boman*, 1993, 1995; *Painter and Paterson*, 1994; *Liu and Molz*, 1996, 1997]. The formulations for these models are based on the stochastic time series where the property of interest varies in one dimension. Both horizontal and vertical ln(K) data have been analyzed for potential fractal behavior from data collected over a variety of field scales. However, the type of stochastic fractal deemed suitable for the data and the power law exponent estimated often vary from site to site as well as from horizontal to vertical directions. Although it is generally agreed that the reason stochastic fractals tend to describe heterogeneity in sedimentary rocks is that stratification tends to occur at various scales [*Painter*, 2003; *Ritzi et al.*, 2004], there is yet a clear explanation of the kind of physical processes that create the "fractal" deposits [*Molz et al.*, 2004].

[3] In a sedimentary environment where ln(K) correlation is scale-dependent, which model is more appropriate? A multilevel model with finite correlation ranges defined for different sedimentary hierarchies, or stochastic fractals for which the correlation range is infinite? These questions are

[1]Department of Geological Sciences, Indiana University, Bloomington, Indiana, USA.
[2]Now at Department of Geological Sciences, University of Michigan, Ann Arbor, Michigan, USA.
[3]Department of Geology and Geophysics, University of Minnesota, Minneapolis, Minnesota, USA.
[4]Earth and Environmental Sciences Division, Los Alamos National Laboratory, Los Alamos, New Mexico, USA.
[5]Chevron Texaco, San Ramon, California, USA.
[6]Department of Earth Sciences, University of New Hampshire, Durham, New Hampshire, USA.

0043-1397/05/2004WR003756$09.00

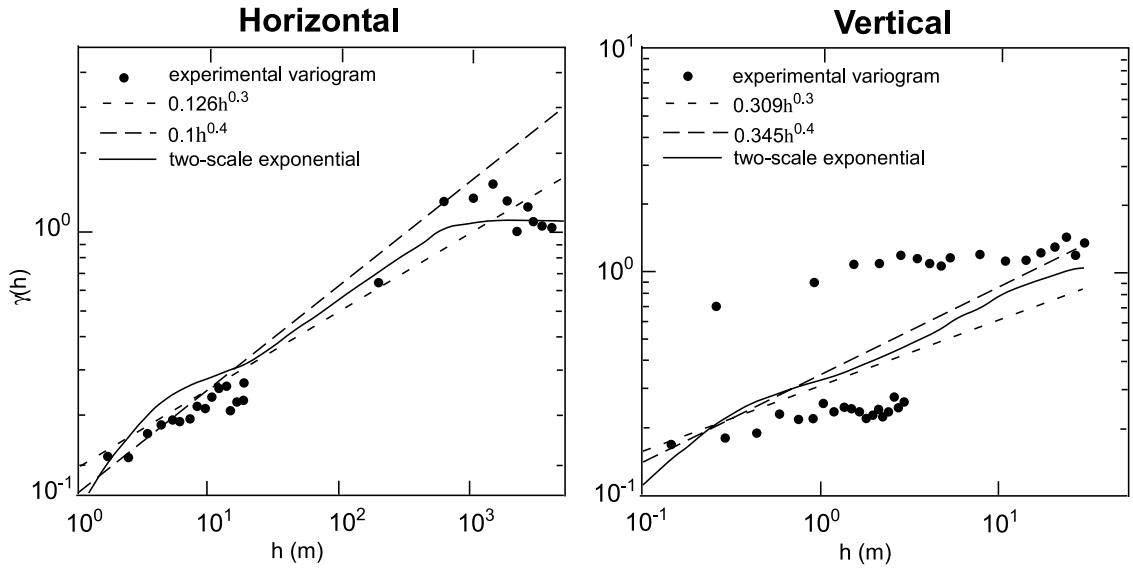

Figure 1. The experimental ln(K) variograms (dots) computed in the horizontal and vertical directions at the Cape Cod site [after *Rajaram and Gelhar*, 1995]. Two power law variogram models and a two-scale exponential model were fit [*Rajaram and Gelhar*, 1995]. Here h is the lag distance in a given direction.

hard to answer given the often large uncertainties in experimental ln(K) variograms constructed from field data. For example, a variogram analysis was conducted on ln(K) measured with borehole flowmeters over a small area (20 m horizontal extent and 7 m vertical extent) and with slug tests over a larger area (5 km horizontal extent and 50 m vertical extent) within relatively well sorted glacial outwash sandstone in Cape Cod, Massachusetts [*Springer*, 1991; *Rajaram and Gelhar*, 1995]. Both horizontal and vertical experimental ln(K) variograms were computed, and in each variogram there appeared two levels of variability where the higher sill corresponded to the slug test data (Figure 1). Two power law variogram models and a two-level exponential model were fit onto the experimental variograms [*Rajaram and Gelhar*, 1995]. Note that the conductivity used to construct the variograms came from two data sets of different support, i.e., slug test versus flowmeter, and the slug test variogram was considered unreliable over short lags [*Rajaram and Gelhar*, 1995]. Combined with the measurement uncertainties associated with each type of data, it is not clear whether these structures truly reflect the natural ln(K) variation at this site. However, compared to most field-based studies, the study described above was based on exhaustive sampling campaigns. This points to the limitation of using outcrop data to understand conductivity heterogeneity and its correlation. To address these issues, a complete knowledge of the ln(K) variations within the deposit is preferred, requiring detailed sampling at large spatial scales incorporating multiple facies types while each local conductivity is measured at a consistent support.

[4] In this study, a geostatistical analysis was conducted on a high-resolution cross-sectional image of a deposit created in an experimental facility where multiple sedimentary facies formed in response to a variety of depositional processes. This image was first scaled up to sedimentary basin dimensions. The image gray scale was then converted to ln(K) based on a set of field-based conductivity endmembers. A synthetic basin-scale hydraulic conductivity map was thus created with similar mean, variance and frequency distribution to a natural fan deposit. For selected regions (or "deposits") of this map representing similar or different depositional environments, experimental ln(K) variograms were computed using the complete conductivity information. Under the alternative assumptions of second-order stationarity and statistical self-affinity, exponential and power law variogram models were fit onto the experimental variograms, respectively. Both an integral scale and a Hausdorff measure (power law exponent; related to the spectral slope) were obtained for each variogram. To determine the directional sensitivity of the Hausdorff measure, for each deposit, a Hausdorff measure was estimated from the major or along-dip variogram, the minor or along-strike variogram, the horizontal variogram, and the vertical variogram. We explore the link between the correlation measures, the sampling domain size and the underlying sedimentary structure. We found that the Hausdorff measure of the deposits lies within a range comparable to that of natural geological deposits. It increases from nonstratified to stratified deposits with a cutoff of around 0.15. It is insensitive to the search direction in the nonstratified deposits. In the stratified deposits, depending on the problem size in relation to the size of the dominant heterogeneity, both the correlation structure and the Hausdorff measure can change. Thus the fractal "signature" of the sedimentary deposits is not only depositional process-dependent but also problem-scale-dependent. On the basis of the observed systematic variations of the variogram structure, the field experimental variograms (Figure 1), and the "scale effect"of the ln(K) correlation range, we proposed a hierarchical variogram with local stationarity for a sedimentary system characterized with stratifications that occur at multiple scales.

2. Experimental Stratigraphy

2.1. Experimental EarthScape Facility

[5] The deposit analyzed in this study was created in the Experimental EarthScape facility (XES) at the Saint Anthony Falls Hydraulics Laboratory, University of Min-

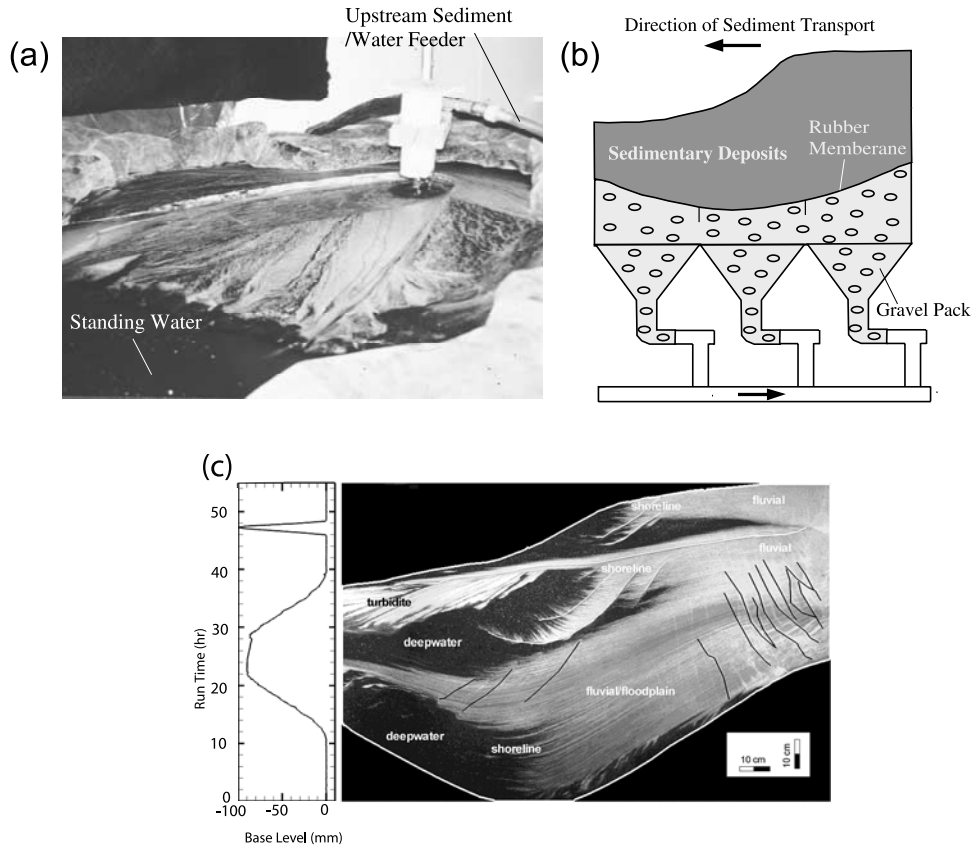

Figure 2. (a) The prototype experimental deposit ($1.6 \times 1.0 \times 0.8$ m^3). Dark and light particles are composed of coal and sand, respectively. At the left edge is standing water, opposite to the upstream sediment/water feeder. (b) A schematic diagram of the system of funnels connected to the tank basement which controls subsidence. Subsidence is induced by firing a pulse of high-pressure water into the elbow pipe, knocking a small volume of gravel into an exhaust line. (c) A cross-sectional stratigraphic image from the prototype experiment. The outline of the deposit is indicated, outside of which there are no data. Major depositional environments are identified along with major faults (black lines) and unconformities (white lines). The left diagram is the imposed "sea level" fluctuations during the experiment. The sandy facies correspond to lower sea levels (regression); the darker facies correspond to higher sea levels (transgression). See color version of this figure in the HTML.

nesota [*Schneider*, 1998; *Paola*, 2000; *Paola et al.*, 2001; *Heller et al.*, 2001]. Using fine quartz sand and coal as proxies for coarse- and fine-grained (clay) sediments, sedimentary packages were generated within a three-dimensional flume fitted with a flexible, subsiding floor. The grain size for the fine quartz sand is nearly uniform at 120 μm; the coal is coarser and poorly sorted. The specific gravity of this sand is 2.65 while that of the coal is 1.3. The coal is not intended to be an exact mechanical analog of a particular size class. The sand-coal mixture is a simple bimodal mixture that displays strong and readily measurable hydraulic sorting by processes analogous to those that produce size sorting in nature.

[6] A prototype experiment was conducted in 1996 creating a 1.6 m long, 1.0 m wide, and 0.8 m thick deposit (Figure 2a). At the onset of the experiment, the tank was filled with pea-size gravel covered by a rubber membrane. From a single source location, a 50:50 mixture of coal and fine quartz sand was introduced into the flume with water. The sediment flux rate was controlled to keep pace with the subsidence rate of the basement (Figure 2b). During the experiment, the elevation of the standing water at the downstream side was varied in a sinusoidal manner to represent eustatic sea level fluctuations in a shallow marine environment ("base level"; Figure 2c). Two sea level cycles were imposed (Figure 2c): during the first 10 hours, the sea level was constant and the shoreline position was near the mid basin; from 10 to 40 hours, the sea level finished a long-period cycle of first dropping and then rising, the shoreline correspondingly first extended to further downstream and then retreated upstream; from 46 to 48 hours, a short-period cycle of more rapid sea level change was imposed, and both shoreline and turbidite deposits formed. Thus, over time, changes in sea level caused large-scale shoreline regression and transgression. Within the flume, sediment transport was dominated by fluvial, shoreline and submarine processes occurring over varying spatial and temporal scales, forming channels and floodplains and creating turbidity currents in the adjacent "sea". At the distal end of the flume, coal particles settled out of the open water as fine-grained clay or silt would settle in an open ocean. Within the fluvial environment, auto cyclic channel switching induced shorefront delta avulsions, while the imposed basement subsidence influenced the patterns of

sediment deposition by allowing faults to develop. The prototype deposit formed in response to the combined forcing of sediment input, basement subsidence, and sea level change; the dominant processes that formed the deposit are comparable to those forming a natural fluvial/deltaic system. A more detailed sedimentological analysis of this experiment is given by *Paola* [2000] and *Paola et al.* [2001].

[7] After the deposit was produced, it was dissected along a face parallel to the average transport direction, 210 mm from the centerline. A high-resolution photograph of the sediment face was taken and digitized (Figure 2c). This two-dimensional image contains 1000 pixels in the horizontal direction and 600 pixels in the vertical direction. A gray scale is associated with each pixel, representing an average light reflection from about 100 sand-sized particles. It varies between 0 and 232, corresponding to the highest coal and sand fractions, respectively. Thus lighter colors correspond to sandy sediments deposited in high-energy subaerial fluvial or submarine mass flow environments; darker colors correspond to sediments with higher proportions of coal deposited in either a floodplain or deepwater setting. This image provides a detailed characterization of the sedimentary heterogeneity within the deposit. Not only is heterogeneity observed to vary at different scales, but the local sedimentary structures (e.g., channel and floodplain deposits, turbidite, deepwater deposits) were created by various depositional processes. The stratigraphic heterogeneity is thus organized within the framework of sedimentary architectures, or structured heterogeneity. Further dissection of the deposit reveals that most of the fluvial sands and floodplain clays are laterally continuous, in the direction perpendicular to sediment transport. This is because sheet flow tended to dominate during the formation of much of the deposit. Thus the image, though two-dimensional, has captured most of the sedimentary heterogeneity of the three-dimensional deposit.

2.2. Basin-Scale ln(K) Map

[8] The experimental deposit has geologically unrealistic dimensions. The bedding angle of the stratified deposit sometimes exceeds 30°, rarely observed in natural sedimentary systems. To ensure a viable dimension/gradient for a hydraulic conductivity map, the stratigraphic image was scaled up to 100 km in the horizontal direction and 3 km in the vertical direction (Figure 3a). This was accomplished by assuming an appropriate length scale for each pixel (Δx = 100 m; Δz = 5 m). The basin dimensions were chosen so that the average topographic slope is 1/100, and the basin length to depth ratio is 50:1, falling within the observed range of natural systems [*Belitz and Bredehoeft*, 1990]. After the image scale-up, the average bedding angle is less than 1°, consistent with the observed regional dip in fluvial/deltaic deposits. Other considerations also prevent direct evaluation of the physical deposit. For example, image scale up is needed to create a hydrologically definable system since a hydraulic conductivity cannot be associated with a single pixel which corresponds to a very small volume of the deposit. This volume is beneath the typical scale of a representative elementary volume (REV) at which hydrological parameters including the hydraulic conductivity are defined [*Bear*, 1972]. For selected deposits, an effective hydraulic conductivity was estimated using a numerical flow method and a Gaussian-based analytic-stochastic model. These analyses also require a real REV size to be associated with each pixel. Although the upscaled dimensions of our basin are somewhat arbitrary, our choice of dimensions is similar to that of *Pratson and Gouveia* [2002] who generated synthetic seismic velocity map based on the XES deposit. It is important to point out that in this study, both the correlation structure of the relative ln(K) variograms and the Hausdorff measure are not affected by the chosen scale-up ratio. This can be easily verified by changing the lag units for the variograms (representing different scale-up ratios) and observing the same correlation structure of the variograms with the same power law slope.

[9] The scaled-up stratigraphic heterogeneity was translated to conductivity heterogeneity based on linear interpolation of the gray scale and two natural log hydraulic conductivity end-members [$\ln(K_{sand})$, $\ln(K_{clay})$]:

$$\ln(K) = \frac{g}{232}\left[\ln(K_{sand}) - \ln(K_{clay})\right] + \ln(K_{clay}) \qquad (1)$$

where g is the gray scale value ($0 \leq g \leq 232$); $\ln(K_{sand})$ and $\ln(K_{clay})$ correspond to the highest and lowest gray scale values, respectively. In essence, equation (1) estimates hydraulic conductivity based on sediment sand/clay ratios. However, equation (1) is nonunique. Other methods have been employed to relate permeability to petrophysical parameters. For example, *Koltermann and Gorelick* [1995] (hereinafter referred to as the KG model) developed an empirical model relating grain size characteristics and packing style to permeability. However, for sand/clay mixtures, our log linear model does an equally good job of matching the permeability data as that of KG model [*Koltermann and Gorelick*, 1995, p. 3291, Figure 6]. In some regards, our model is more realistic. For example, when the porosity of the coarse-grained sediments is less than 0.25, the KG model predicts increasing permeability with increasing clay content which is counterintuitive. It is also worth noting that our approach of relating image gray scale to log permeability is not new. *Tidwell and Wilson* [2002] found that the spatial structure of natural log permeability is strongly correlated to that of the digital gray scale image of the respective rock face. Their permeability was obtained with thousands of centimeter-scale minipermeameter measurements, indicating that visual image of rock faces can be used to delineate the spatial pattern of local (log) conductivity variations.

[10] With equation (1), only one ln(K) value is interpolated from each pixel gray scale. We thus assume that each scaled-up pixel represents a local-scale, homogenous, and isotropic porous media upon which a local hydraulic conductivity is defined. The selection of the hydraulic conductivity end-members is based on an unconsolidated alluvial fan deposit in the Livermore Valley of California [*Lu et al.*, 2002]. Hydraulic conductivity measurements at this site indicate a multimodal frequency distribution with 4 major facies groups: floodplain, levee, debris flow and channel (Figure 3b). Each facies group has a ln(K) distribution that is approximately normal; ln(K) (in m/d) from all facies has a range of −6 to 1.75. Accordingly, these values were selected as the conductivity end-members for

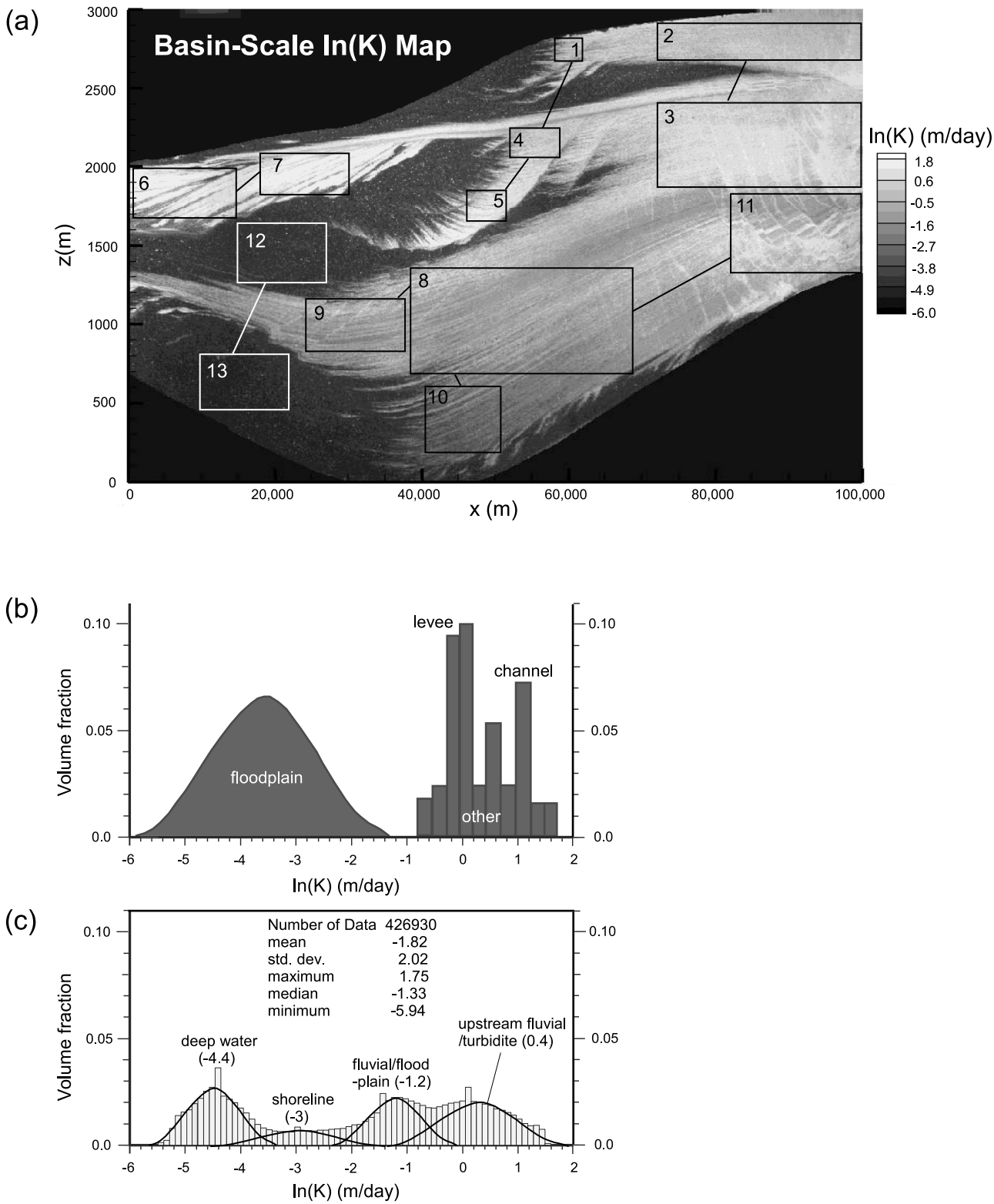

Figure 3. (a) An interpolated basin-scale ln(K) map (in m/d) based on equation (1). The locations of the sampled regions are indicated as well as the sample ID. Deposits created in similar depositional environment are linked by lines. (b) The ln(K) (m/d) frequency distribution based on measurements from an alluvial fan (after *Lu et al.* [2002], with kind permission of Springer Science and Business Media). (c) ln(K) frequency distribution of Figure 3a along with summary statistics. Four lognormal populations were identified, superimposed with four normal density curves with the mean ln(K) in parenthesis.

equation (1). After the image interpolation, a synthetic ln(K) map was created for which a global ln(K) histogram was also constructed (Figure 3c). Compared to the fan deposit, this map is also multimodal with four approximately normal distributions. Although each population of the fan deposit corresponds to a distinct facies, the experimental deposit demonstrates a more mixed frequency distribution. Compared to the fan deposit, a wider range of depositional processes was represented in the experimental deposit. Nevertheless, both sedimentary systems were created by multiple depositional processes, be it at an experimental flume scale or at the natural scale of an alluvial fan. Both systems have a multimodal ln(K) distribution with each mode likely characterized by a normal density. Although the sediment transport processes in both systems may be at times chaotic, some intrinsic and fundamental processes are at work that give rise to such material distribution.

[11] This approach of assigning petrophysical parameters based on image gray scale and typical end-member property of sand and clay was also adopted by *Pratson and Gouveia* [2002]. In this study, the hydraulic conductivity of the sand and coal used in the experiment is around 10^{-6} m/s and 10^{-3} m/s, respectively, corresponding to the conductivity range of fine to medium sand [*Freeze and Cherry*, 1979]. If these values were chosen as the end-member conductivity, the synthetic map would become too permeable compared to natural sand/clay systems (e.g., the fan deposit has an approximate conductivity range of 10^{-4} to 10^{-8} m/s). More importantly, the conductivity map would be opposite to a natural system, i.e., the darker deposits representing clay would be more permeable than the sandy deposits. Note that in Figure 3c, the low-conductivity distributions correspond to the more distal deposits with higher "clay" content. After the image interpolation, the synthetic map displays overall univariate characteristics (the extreme, the mean, and the spread of ln(K)) comparable to the fan deposit. The standard deviation of ln(K) is 2.02, falling within the observed range [0.4, 4.0] of geological media [*Gelhar*, 1993, p. 2].

[12] In summary, the scale-up of an image of the XES deposit to sedimentary basin dimensions and the conductivity interpolation based on image gray scale and a chosen set of conductivity end-members have produced a basin-scale ln(K) map with geologically realistic dimensions and gradients. It preserves all scales of the structured stratigraphic heterogeneity, while each local conductivity is defined over a consistent data support. Ln(K) of this map has a variability range and frequency distribution comparable to a natural alluvial fan. Within a hierarchical framework each depositional environment in this map can be characterized as a geological formation within which distinct facies or facies assemblages exist. For example, if the fluvial/floodplain deposit is characterized as a terrestrial fluvial formation, the individual sand and clay units can be characterized as fluvial and floodplain facies, respectively (Figure 2c). The thicker, sand-rich units of the turbidite deposit can be characterized as submarine mass flow facies, while the interbedded clay characterized as deepwater facies. The ln(K) map is also statistically heterogeneous, i.e., the ln(K) mean, variance, and correlation structure change as the depositional environment changes. This natural log conductivity map is the foundation for the geostatistical analysis presented below.

3. Geostatistical Analysis

3.1. Data Sampling and Univariate Analysis

[13] Both univariate and bivariate analyses were conducted on 13 selected regions of the ln(K) map, each region was selected from a distinct depositional environment (Figure 3a). Each region or sample is rectangular and of varying sizes. The size was selected to be as large as possible without crossing into a different depositional environment. Samples 1, 4, 5 represent the shoreline deposits created during episodes of marine transgression. Samples 2 and 3 represent the upstream fluvial deposits that are predominantly sandy. Compared to sample 2, sample 3 is weakly stratified as well as populated with some high-K faults. Samples 6 and 7 are part of turbidite deposits created during the last sea level rise. Samples 8, 9, 10 represent the downstream fluvial/floodplain deposits. Sample 11 represents the upstream fluvial/floodplain deposits that are extensively faulted. Samples 12 and 13 represent low-energy deepwater deposits. For each sample, the mean and variance of ln(K) were computed and the ln(K) normality was tested with a Kolmogorov-Smirnov test. The normality test was conducted on random subsets of each sample at 95% confidence interval. Since random sampling does not preclude correlated data, multiple tests were conducted, each selecting a different subset randomly. Whether data pass the normality test was determined by the expected outcome. Note that although the entire ln(K) map is statistically heterogeneous, locally within a depositional environment, the material property is approximately statistically homogeneous. For most samples, the ln(K) variance is less than 1.0 (see section 4), within the range of applicability for the perturbation-based stochastic theories to estimate the effective properties. Each sample representing a particular depositional environment incorporates only one or two facies types of either sand-rich or clay-rich units. The normality test is necessary since the selected analytic-stochastic theory for the estimation of effective conductivity requires that the local conductivity is lognormally distributed (see section 5).

3.2. Variogram Analysis

[14] To characterize ln(K) spatial correlation, an experimental variogram map was computed for each sample using GSLIB program *varmap* [*Deutsch and Journel*, 1992]. The variogram map was used to indicate the possible existence of statistical anisotropy in a sample, and if it exists, to further identify the directional angle of the statistical axis. Using GSLIB *gamv* program, two directional variograms were then computed along the major/minor statistical axes which correspond to the directions of maximum/minimum ln(K) continuity, respectively. Note that since many of the samples are stratified, the direction of the maximum continuity is usually along the bedding plane. The experimental variograms constructed along this direction are referred to as major or along-dip variograms, while those perpendicular to bedding (minimum continuity) are referred to as minor or along-strike variograms. Using GSLIB *gam* program, two additional directional variograms were computed along

the horizontal/vertical coordinate axes; these variograms are thus the horizontal/vertical variograms. Following the angle convention in GSLIB, we use "azimuth" to indicate the angle between the search direction and the vertical axis (z). Note that in the directional variograms, the unit lag distance is chosen to be approximately the data spacing for a given direction. The maximum lag distance is chosen to be half of the sample domain length scale, eliminating any "edge effects" due to large-scale trends which would not be representative of the correlation structure in the sample (A.G. Journel, personal communication, 2003). For the major variograms, the search strategy utilizes a high angular tolerance (45°) and a narrow bandwidth (usually around unit sand/clay thickness) [*Englund and Sparks*, 1988]. This ensures that more data pairs could be found at smaller lags to reduce the nugget effect near the origin while the variogram shape is distinguished by preventing too much data mixing across facies types. Moreover, given the large number of data points for each sample, each variogram estimate is computed from a few hundred data pairs to up to tens of thousands of pairs, the coefficient of variation of each estimate is small, thus no confidence interval is computed. Both the variogram map and the directional variograms are also normalized by the sample variance (s^2), which is identified by a line at 1.0 in the directional variograms. Note that although s^2 is often used as an estimator for the variogram sill (theoretical population variance σ^2), s^2 in general underestimates the sill in a stationary random field (SRF), especially if the data are collected over an area smaller than the correlation range [*Chilès and Delfiner*, 1999]. Therefore, if an experimental variogram displays a sill, it is used as the estimator for σ^2 rather than using the sample variance. Following conventional practice, the sample variance is but a convenient choice to construct the relative variograms.

[15] Two variogram models are fit onto each experimental variogram: an exponential function assuming SRF; a power law function assuming nonstationary, self-affine RF. The exponential variogram model is commonly given as

$$\gamma(h) = C_0 + C_1[1 - \exp(-h/\lambda)] \tag{2}$$

$\gamma(h)$ is the directional variogram; h and λ are the lag separation and integral scale along a given direction, respectively. C_0 is a "nugget effect" to model the variogram discontinuity near the origin. C_1 is a model coefficient. The model sill is $C_0 + C_1$, used for estimation of σ^2. Note that the model parameters reported in this study are relative to the sample variance, e.g., C_0/s^2, C_1/s^2. The nugget effect may occur due to either measurement errors or existence of small-scale variability beneath the sampling grid (e.g., sample spacing > correlation range of the conductivity "microstructure") [*Chilès and Delfiner*, 1999]. The power law variogram model characterizes a self-affine stochastic fractal and is often given as:

$$\gamma(h) = c \cdot h^{2H} \qquad (0 < H < 1) \tag{3}$$

c is a constant, H is the Hausdorff measure. Applying a scaling factor (s) to lag separation, $\gamma(s \cdot h) = s^{2H} \cdot \gamma(h)$, the power law variogram model is thus scale-invariant. This means that the variogram functions at different problem scales have a similar "appearance" when subjected to appropriate renormalization. The power law variogram further plots as a straight line in a log-log plot, therefore a characteristic length cannot be associated with it. The Hausdorff measure is used to characterize the long-term persistence of a stochastic fractal [*Turcotte*, 1997]: when $0 < H < 0.5$, the increment of the process is negatively correlated or antipersistence (e.g., increase in property values tends to be followed by a decrease, vice versa); when $0.5 < H < 1$, the increment is positively correlated or persistence (e.g., increase tends to be followed by further increase); when $H = 0.5$, the increment becomes uncorrelated white noise. The magnitude of the Hausdorff measure thus indicates the ln(K) correlation characteristics, e.g., whether ln(K) tends to change over space or noisy data (antipersistence) or remains relatively smooth (persistence). Moreover, if a one-dimensional process is a stochastic fractal, its spectral density S(k) has a power law dependence on the wave number k [*Turcotte*, 1997]

$$S(k) \propto k^{-\beta} \tag{4}$$

β is referred to as the spectral slope and is related to the Hausdorff measure via

$$\beta = 2H + 1 \tag{5}$$

Like the Hausdorff measure, the magnitude of spectral slope indicates the smoothness or roughness of a series. As the spectral slope increases, ln(K) series becomes smoother. Since physical properties are usually defined over a finite range of scales, stochastic fractals are also bounded. This is reflected in a spectral density that is distributed over a finite range of wave numbers $[k_{min}, k_{max}]$: k_{min} corresponds to domain size cutoff; k_{max} corresponds to sample spacing cutoff.

[16] Although one of our reviewers suggested that we conduct an indicator variogram analysis in association with a hierarchical decomposition [e.g., *Ritzi et al.*, 2004], in the current study, we present the results of the continuous ln(K) variogram analysis for several reasons: (1) For a hierarchical analysis, artificial cutoff values have to be employed to turn the continuous ln(K) map to an indicator map, e.g., facies type. The hierarchical analysis requires the estimation of facies proportions, local subunit statistics, and transition probabilities. These statistics would be difficult to estimate given our numerous sand/clay stratifications while each strata is often very thin. (2) We investigate the impact of problem size on ln(K) correlation characteristics whereby the observed systematic change in the correlation measures (variogram structure, Hausdorff measure) gives hints to what kind of behavior may arise given a finite sampling domain. To compare the spectral slope of the ln(K) map with that of natural deposits, the continuous ln(K) variogram is also needed. (3) The variance and correlation range of the continuous ln(K) variogram are used to infer effective hydraulic conductivity for selected deposits with a Gaussian-based analytic-stochastic model. To our knowledge, there are no theories that can predict effective conductivity based on results from a hierarchical analysis. (4) The hierarchical identity developed by *Ritzi et al.* [2004] is verified by constructing continuous ln(K) variogram, so the analysis conducted herein is a necessary component of the indicator-based hierarchical

Table 1. Results of the Kolmogorov-Smirmov Normality Test Conducted on Random Subsets of Each Sample[a]

Sample	Test 1[b]	Test 2	Test 3	Test 4	Test 5	Test 6	Test 7	Test 8	Test 9	Test 10	Expected Outcome	Comments
1	0	0	1	0	1	1	0	0	0	1	0.4	normal
2	0	0	0	0	0	0	0	1	0	0	0.1	normal
3	0	0	0	0	0	0	0	0	0	1	0.1	normal
4	1	0	1	0	1	1	0	0	1	0	0.5	inconclusive
5	1	1	1	1	1	1	1	1	1	1	1	nonnormal
6	1	1	1	1	1	1	1	1	1	1	1	nonnormal
7	1	1	1	1	1	1	1	1	1	1	1	nonnormal
8	0	0	0	0	0	0	0	0	0	0	0	normal
9	1	0	0	0	0	0	0	0	0	0	0.1	normal
10	0	0	0	0	0	0	0	0	0	0	0	normal
11	0	0	0	0	0	0	0	0	0	0	0	normal
12	1	1	1	1	1	1	1	1	1	1	1	nonnormal
13	0	1	1	1	1	0	0	1	0	0	0.5	inconclusive

[a]The subset size is 100 for all samples. For each sample, the test was repeated 10 times, each time drawing a different subset randomly.
[b]Null hypothesis: ln(K) comes from a normal distribution; if 0, do not reject the null hypothesis at significance level 5%; if 1, reject the null hypothesis at significance level 5%. Using 0.5 as a cutoff for the expected outcome of the test, the normality test is considered passed for the outcome less than 0.5; not passed for outcome greater than 0.5; inconclusive if the outcome is equal to 0.5.

analysis. Such an analysis can be the subject of a follow-up study.

4. Results

4.1. Univariate Analysis

[17] The normality test conducted on each sample ln(K) field indicates that for the given sample size, fluvial and fluvial/floodplain deposits pass the test while the shoreline (sample 5), turbidite (samples 6 and 7) and deepwater deposits (sample 12) fail the test (Table 1). While the histogram of the turbidite deposit tends to be bimodal, the deepwater deposits have positive skews, distinctively different from the rest of the sandy deposits with zero to negative skew (not shown). Transport into the "ocean" basin and the subsequent settling of a small amount of sands is presumed to be responsible. The faulted fluvial/floodplain deposit of sample 11 consistently passes the test despite the fact that it is intersected by extensive high-conductivity faults. Moreover, the univariate characteristics of the selected samples can be expected to be scale-dependent. *Ritzi et al.* [2004] presented a schematic diagram showing a hypothetical fluvial point bar deposit. Their bimodal ln(K) histogram at the "fluvial assemblage" scale evolved into a multimodal distribution when an entire depositional system was incorporated, not unlike the comparison of the bimodal turbidite to the global ln(K) histogram which contains several normal populations (Figure 3c).

4.2. Exponential Model/Stationary RF

[18] Assuming second-order stationarity for each sample, an exponential model was fit to the first structure (leveling off) of the major and minor variograms (Figure 4). An integral scale is obtained which is the lag separation when the normalized covariance is e^{-1}. The sample domain size, the associated depositional environment and the exponential model parameters are listed in Table 2. Most of the samples display statistical anisotropy (correlation range in one direction is longer than the other), while the azimuth angle of the major statistical axis reflects the average angle of the bedding plane within a sample. In general, the integral scales estimated along the major axis (λ_{max}) are orders of magnitude greater than those estimated for the minor axis (λ_{min}). The statistical anisotropy ratio ($\lambda_{max}/\lambda_{min}$) ranges from 35 $\sim$ 77 (fluvial), 100 $\sim$ 240 (shoreline), to 150 $\sim$ 500 (fluvial/floodplain), generally comparable to those estimated from natural sedimentary rocks [*Deutsch*, 2002]. Note that the two-dimensional image used for this analysis cuts through the fluvial channels and shoreline deposits. This may result in apparently separate or discontinuous units, masking any three dimensional processes (e.g., channel switching; delta front avulsion). For some deposits, the statistical anisotropy ratio may be higher if a three-dimensional ln(K) map can be constructed, although a variogram analysis may fail to capture such nonlinearity [*Caers and Zhang*, 2004]. In contrast, the deepwater deposits have the shortest integral scales and model fitting returns a statistical anisotropy ratio of 20, equivalent to the scale-up ratio ($\Delta x/\Delta z$ = 20). The original experimental-scale deepwater deposits are thus isotropic, which is linked to the direction-independent depositional style of coal settling. Compared to natural deepwater deposits which often have high statistical anisotropy ratio (80 $\sim$ 350) [*Deutsch*, 2002], the experimental deposit has characteristics of a recently formed unconsolidated system. Similarly, dividing the anisotropy ratio by the scale-up ratio, we can determine the statistical anisotropy in the original deposit as 2 $\sim$ 4 for fluvial deposits, 2 $\sim$ 12 for shoreline deposits, and 7.5 $\sim$ 25 for fluvial/floodplain deposits. Clearly, such ratios are rarely seen in natural fluvial/deltaic systems, image scale-up is thus a natural choice to create a ln(K) map with statistically realistic properties.

[19] The above analysis evaluates the directional variograms along the major/minor statistical axes of anisotropy. However, in field investigations, the dominant sedimentary structure is often beyond direct observation and the actual bedding angles may be less certain. Coupled with data scarcity, a variogram map is rarely useful to identify the statistical axes. Since sedimentary deposits usually have low incline, it is common practice to compute the major variograms along the horizontal direction and the minor variogram along the vertical direction [e.g., *Sudicky*, 1986; *Rehfeldt et al.*, 1992; *Desbarats and Bachu*, 1994; *Rajaram and Gelhar*, 1995]. If the bedding plane is perfectly level, the horizontal variogram will usually correspond to the direction of maximum correlation. However, if the bedding

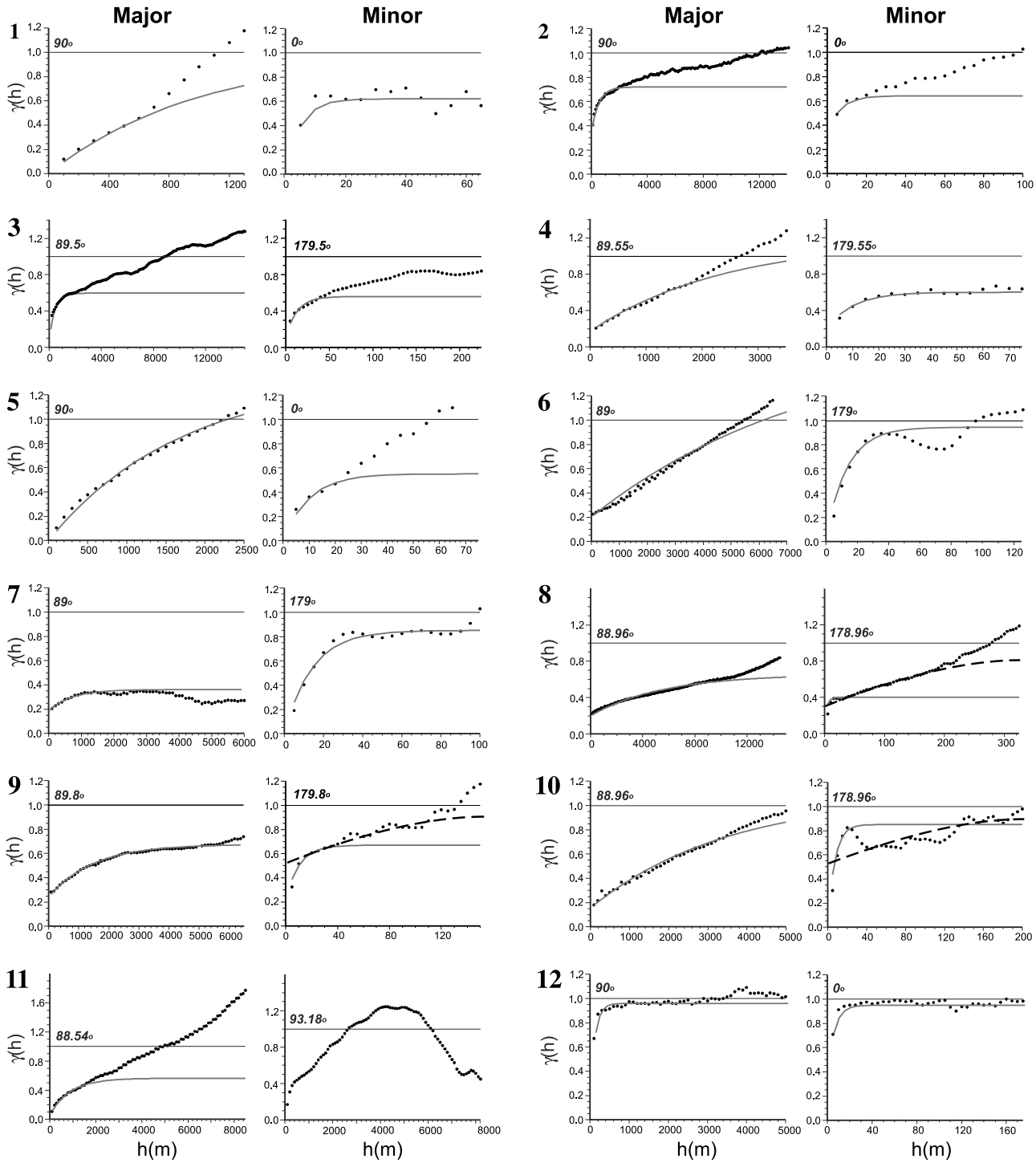

Figure 4. The experimental relative ln(K) variograms (dots) computed along the major and minor statistical axes for samples 1 ∼ 12: shoreline (1, 4, and 5), upstream fluvial (2 and 3), turbidite (6 and 7), fluvial/floodplain (8, 9, 10, and 11), and deep water deposit (12). The azimuth angle of each variogram is indicated. An exponential model (curve) is fit onto each variogram with model parameters listed in Table 2. For the minor variograms of samples 8, 9, and 10 a large-scale exponential model is also fit (dashed curve). For sample 11, 88.54° indicates average bedding angle; 93.18° indicates average fault orientation.

plane is inclined as in most fluvial/deltaic environments and the problem scale is large, how representative is the horizontal variogram of the actual major variogram? To provide some insights, both the horizontal (azimuth = 90°) and the major (azimuth = 88.96°) variograms were computed for sample 8, using *gam* and *gamv* programs, respectively (Figure 5a). Though the difference in search angle is small, the horizontal variogram shows nested structure due to the

Table 2. Geostatistical Characteristics of ln(K) Tabulated for All Samples[a]

Depositional Environment	ID	L_x, m	L_z, m	Univariate Characteristics	s^2	Major Variogram				Minor Variogram		
						Nugget (C_o)	Azimuth, deg	C_1	λ_{max}	C_1	λ_{min}	$\lambda_{max}/\lambda_{min}$
Shoreline	1	2600	130	normal	0.48	0.00	90.00	1.00	1000.0	0.62	10.0	100
Shoreline	4	7100	155	inconclusive negatively skewed	0.41	0.18	89.55	1.00	2400.0	0.40 (C_o = 0.2)	10.0	240
Shoreline	5	5100	130	nonnormal negatively skewed	0.52	0.00	90.00	1.35	1700.0	0.55	10.0	170
Fluvial	2	28100	205	normal	0.11	0.34	90.00	0.38	517.0	0.30	6.7	77
Fluvial	3	30100	455	normal	0.15	0.12	89.50	0.50	450.0	0.44	13.0	35
Turbidite	6	14100	255	bimodal	1.28	0.10	89.00	1.75	8000.0	0.90 (C_o = 0.05)	13.3	600
Turbidite	7	12100	205	bimodal	0.77	0.18	89.00	0.20	700.0	0.85 (C_o = 0)	14.0	50
Fluvial/floodplain	8	30100	655	normal	0.38	0.10	88.96	0.33	1500.0	0.20	5.0	300
Fluvial/floodplain	9	13100	305	normal	0.30	0.25	89.80	0.44	1500.0	0.47 (C_o = 0.2)	10.0	150
Fluvial/floodplain	10	10100	405	normal	0.35	0.15	88.96	0.94	3500.0	0.85 (C_o = 0)	7.0	500
Fluvial/floodplain with faults	11	17100	455	pass normality test	0.60	0.10	88.54	0.50	883.3	0.61 (C_o = 0)	20.0	44
Deepwater	12	10100	355	nonnormal positively skewed	0.11	0.40	90.00	0.55	120.0	0.55	6.0	20
Deepwater	13	10100	405	inconclusive positively skewed	0.07	0.40	90.00	0.38	130.0	0.38	6.5	20

[a]Sample size (L_x, L_z), associated depositional environment, univariate characteristics, sample variance (s^2), major statistical axis in azimuth angle, integral scales (λ_{max} and λ_{min}) estimated along the major/minor axis, and statistical anisotropy ratio ($\lambda_{max}/\lambda_{min}$). The major axis is determined from variogram map (not shown); the minor axis is orthogonal to the major axis. Both the nugget (C_o) and the sill ($C_o + C_1$) are relative to the sample variance. Note that only C_o for the major variogram is listed; C_o for the minor variogram is equal to C_o of the major variogram unless indicated in parentheses.

incorporation of data pairs of mixed facies types, i.e., the horizontal plane intersects the sandy and clayey units by 1°. The major variogram is more exponential-type for lag distances less than 10 km; it deviates from the exponential shape at larger lags, possibly due to large-scale data mixing, i.e., on average, data pairs separated by 10 km or greater do not belong to the same facies type. Both the vertical (azimuth = 180°) and the minor (azimuth = 178.96°) variograms were also computed for sample 8 (Figure 5b). The two variograms are nearly identical since data variability is similar along the vertical direction and the minor axis. It is of further interest to notice that the vertical and minor variograms have an overall shape that is becoming similar to the major variogram. This indicates that the Hausdorff measure obtained for the vertical/minor variograms would become similar to that of the major variogram (see section 4.3).

4.3. Power Law Model/Self-Affine RF

[20] Under the assumption of a nonstationary, self-affine RF, the power law variogram model was fit to the major, horizontal, minor and vertical experimental variograms and a Hausdorff measure (H) is estimated for each directional

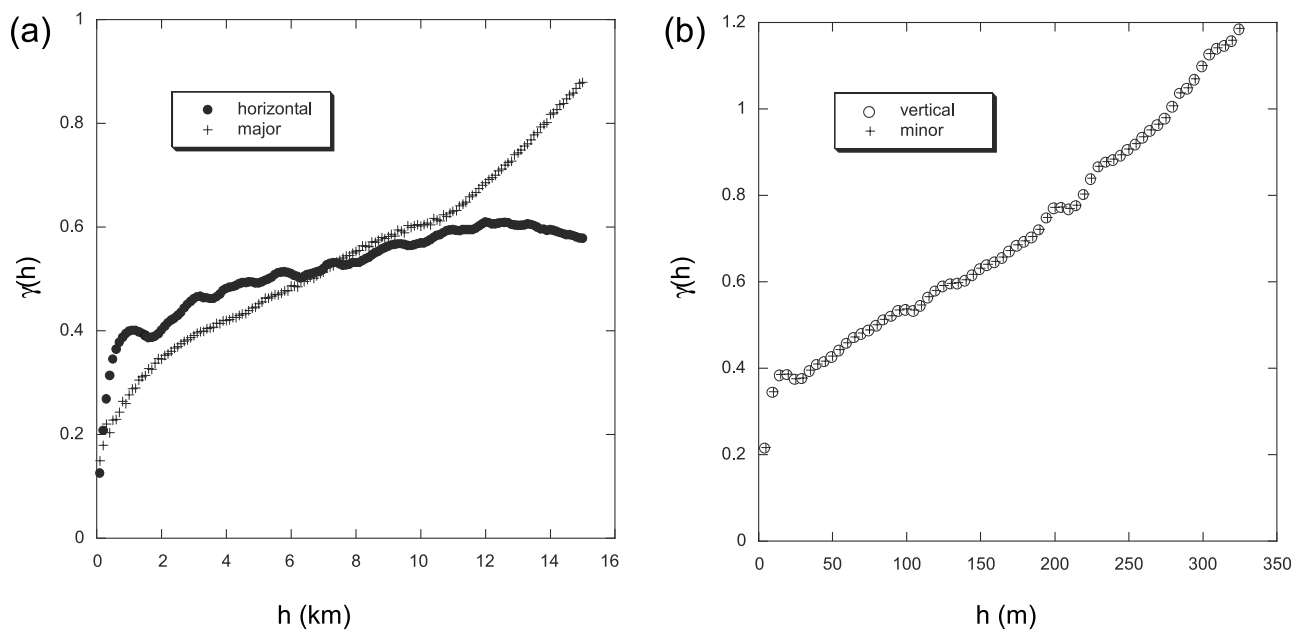

Figure 5. (a) Experimental relative variograms of sample 8 computed along the horizontal and the major axes and (b) along the vertical and the minor axes.

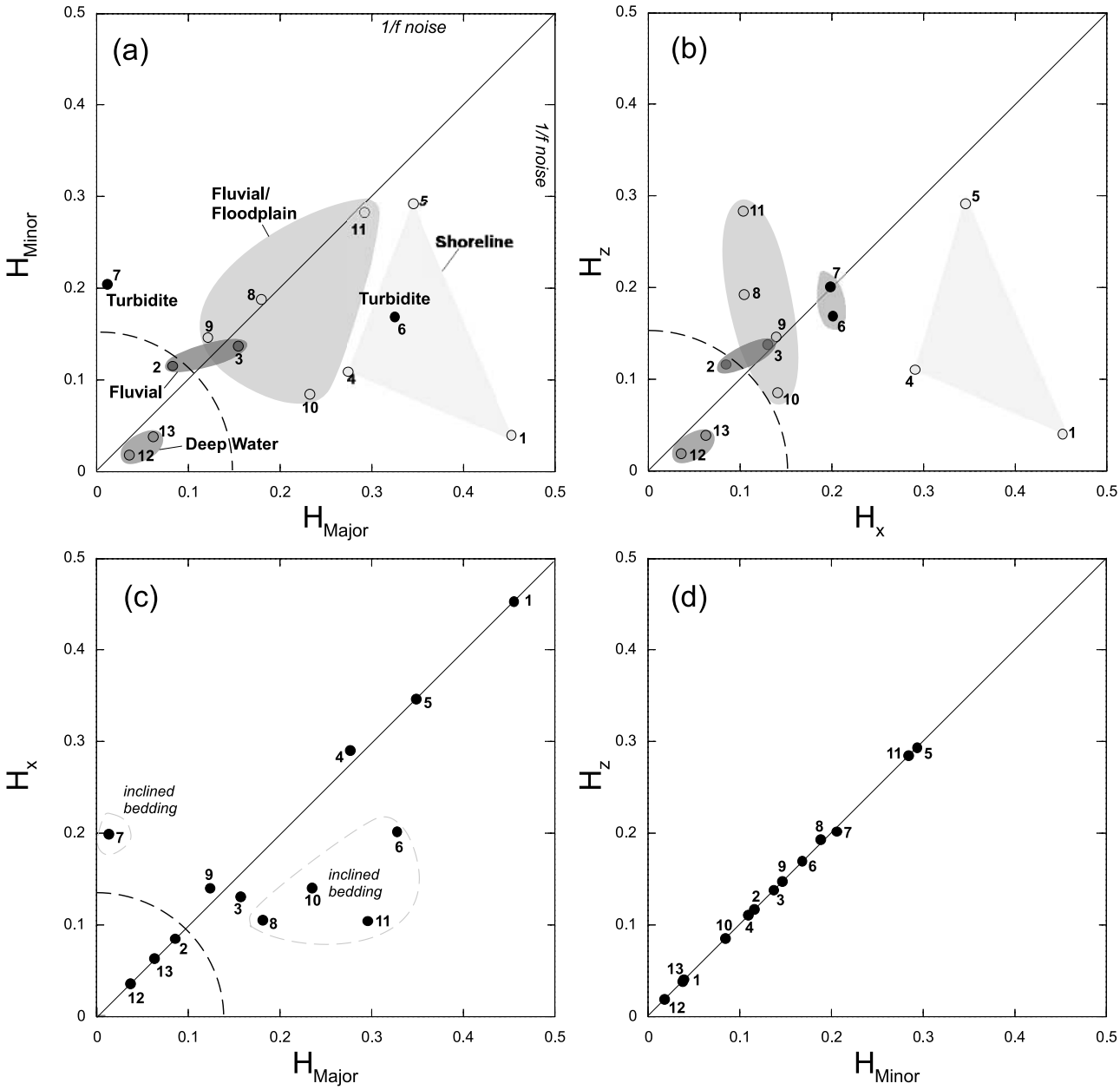

H	rock type	location	direction	reference
0.22	sandstone	Alberta Basin	horizontal	Desbarats and Bachu, 1994
0.34	sandstone	Mobile, AB	vertical	Molz and Boman, 1995
0.39	fluvial sands	Savannah River site, SC	vertical	Liu and Molz, 1996
0.25	hypothetical “juxtaposition” of different media		-	Neuman (1990, 1994)

Figure 6. Scatterplots of the Hausdorff measure estimated for each sample along the (a) major (H_{Major}) and minor (H_{Minor}) statistical axes, (b) horizontal (H_x) and vertical (H_z) coordinate axes, (c) major and horizontal axes, and (d) minor and vertical axes. In Figures 6a and 6b, samples of similar depositional environment are coded with similar shades of gray. The Hausdorff measure of ln(K) in other sedimentary deposits are tabulated along with the references.

variogram by least squares fit. To be consistent with the exponential model fitting which assumes a nugget effect if there is discontinuity of the variogram structure at the origin, the power law variogram was fit to the first nonzero lag, thus also assuming nugget effect if discontinuity exists at the origin. To compare the difference between the Hausdorff measure estimated along the different axes, we constructed 4 scatterplots: H_{minor} versus H_{major} (Figure 6a), H_z versus H_x (Figure 6b), H_x versus H_{major} (Figure 6c), and H_z versus H_{minor} (Figure 6d). Note that for nonstratified

deposits (samples 2, 12, and 13), the statistical major/minor axes generally coincide with the x/z axes; for the stratified deposits, the statistical axes can differ from the coordinate axes by a small angle (samples 6, 7, 8, 10, and 11) or can be nearly colinear with the coordinate axes (samples 3, 9, 1, 4, and 5). Interesting insights are gained from such comparisons and are summarized in the following paragraphs.

[21] For all samples, the range of H is [0.01, 0.45] along the major axis, [0.04, 0.45] along the horizontal axis, [0.02, 0.29] along the minor axis, and [0.02, 0.29] along the vertical axis. The magnitude of the H is less than 0.5 in all directions, indicating ln(K) antipersistence, thus the increment of ln(K) is negatively correlated. These ranges are consistent with the values of H reported from field studies on different geophysical or petrophysical properties of sedimentary rocks which are generally less than 0.5 [*Painter*, 2003]. Note that a Hausdorff measure of 0.25 is a value reported by *Federico and Neuman* [1997] and *Painter* [2003] as typical for sedimentary rocks. Using equation (5), the spectral slope of the selected samples has a range of [1.02, 1.9], falling within the upper range of the 1/*f* noise (0, 2) [*Mandelbrot*, 1983]. Moreover, H of the deepwater deposits is less than 0.1 in all directions, smallest among all samples. As H increases, the depositional environment changes from deepwater ($H < 0.1$), to fluvial ($0.1 < H < 0.2$), to fluvial/floodplain and turbidite ($0.2 < H < 0.3$), while the largest H is generally found in the shoreline deposits. The sedimentary structure in these deposits also changes from little or no structure to the more stratified configurations with a cutoff Hausdorff measure identified at 0.15. Note that compared to the same fluvial deposit of sample 2, the weakly stratified, fault-intersected sample 3 has higher H in both directions and fall outside the cutoff circle (the dashed curve with radius of 0.15). The turbidite deposit of sample 7 has a H_{major} that is very small compared to H_{minor}. Visual inspection reveals that most of this sample is composed of thick sandy beds within which ln(K) is nearly uniform. Thus, along the bedding plane, data pairs are becoming similar and the within-unit variability dominates the overall variance. Along the minor axis, between-unit data variability corresponding to the transition between sand and clay dominates, thus ensuring a H_{minor} that is greater than 0.15. The overall position of sample 7 still falls outside the cutoff circle. However, why would the stratified deposits have higher Hausdorff measure than the nonstratified deposits along one or both directions? This may be explained by their variance distribution since the magnitude of H indicates how the total ln(K) variance is distributed over the wave number space. For a given deposit, the larger the H, the greater the spectral slope, the faster the spectral density decays over the wave number space and consequently the variance of the process is distributed more over the relatively small wave numbers. This indicates that long-range fluctuations are the dominant variability, consistent with the stratified deposits analyzed which have H greater than 0.15. On the other hand, the deepwater and fluvial deposits (samples 12, 13, and 2) have a spectral density distributed more over the larger wave number, thus short-range fluctuations contribute more to the global variance. Indeed, these deposits are characterized by local variability and lack of significant stratification. However, comparison between H_{minor} and H_z reveals that a cutoff Hausdorff measure can no longer be distinguished between nonstratified and stratified deposits, although the deepwater deposits still cluster near the lowest Hausdorff measure (Figure 6d).

[22] A 45° line was drawn through all scatterplots to investigate the sensitivity of the Hausdorff measure with direction. We first look at the Hausdorff measure along and perpendicular to the bedding plane (Figure 6a). For the nearly homogenous deposits (samples 12, 13, 2, and 3), H_{minor} is close to H_{major}, consistent with the findings of *Tubman and Crane* [1995]. Since data variability is not significantly different along either direction, this ''isotropy'' in Hausdorff measure is expected. For the stratified deposits, with the exception of sample 7, some of the points fall near the 45° line (samples 8, 9, and 11) while others fall beneath the 45° line (samples 1, 4, 5, 6, and 10). Note that samples 1, 4, 5, 6, 10 are characterized with a smaller lateral problem size compared to the dominant size of heterogeneity, i.e., average length of sand/clay unit. For these deposits, $H_{minor} < H_{major}$, indicating ''noisier'' behavior along-strike than along dip. The samples whereby the problem size is generally large compared to the dominant size of heterogeneity (samples 8, 9, and 11), the vertical variability becomes similar to the lateral variability. This points to the intriguing possibility that for stratified deposits, the directional sensitivity of the Hausdorff measure is problem-scale-dependent. For example, both sample 8 and sample 10 were created in the fluvial/floodplain environment, and when the problem size grows large compared to the size of the dominant heterogeneity (sample 10 => sample 8), the along-strike Hausdorff measure (H_{minor}) approaches the along-dip Hausdorff measure (H_{major}). In a corresponding variogram analysis, the ''zonal anisotropy'' would approach the ''geometrical anisotropy'', e.g., the variograms constructed for sample 8 along and perpendicular to bedding are becoming similar (Figure 5).

[23] Along the horizontal and vertical axes, the nearly homogenous deposits (samples 12, 13, 2, and 3) again fall near the 45° line while the positions of the samples 6, 7, 8, 10, 11 have changed compared to Figure 6a (Figure 6b). Note that sample 8 has moved away from the 45° line while sample 10 has moved close to it. The turbidite samples also moved close to the 45° line. These changes are a result of the difference between H_{major} and H_x (Figure 6c). This scatterplot shows that most of the samples fall along the 45° line. These are either nonstratified deposits (samples 2, 12, 13) or stratified deposits with a bedding plane either colinear or nearly colinear with the horizontal plane (samples 3, 9, 1, 4, and 5). Thus it is no surprise that their Hausdorff measure along the horizontal direction is similar to that along the major axis. The ones that deviate from the 45° line are samples 6, 7, 8, 10, and 11. These deposits are the stratified deposits with inclined bedding, thus the major axis is not colinear with the horizontal plane and the corresponding correlation characteristics would be different. For example, the horizontal variogram of sample 8 is characterized with multiple nested structures from mixing of data pairs of different facies types at all lag separations (Figure 5a). With the exception of sample 7, samples 6, 8, 10, 11 have $H_{major} > H_x$. This may be explained by the fact that data variability along the bedding plane is dominated

by the long-range fluctuation of the sand or clay units. Along the horizontal direction, data are much "noisier", reflecting the fact that data pairs come from mixed facies types at relatively short lag spacings. Indeed, in Figure 5a, if we fit an exponential model to both variograms, the integral scale of the major variogram is longer than that of the horizontal variogram. Finally, since the data pairs along the vertical direction experience similar variability as data pairs along the minor axis, H_{minor} and H_z fall along the 45° line for all samples (Figure 6d).

[24] In summary, a Hausdorff measure of 0.15 (a spectral slope of 1.3) may identify a cutoff between nonstratified and stratified deposits. However, such cutoff may not be apparent if only vertical data is available. For nonstratified, nearly homogenous deposit, the Hausdorff measure is also direction-independent. For stratified deposit, if the lateral problem size is small compared to the extent of the bedding layers (common cause of "zonal anisotropy"), H_{minor} tends to be smaller than H_{major}, indicating "noisier" behavior along strike. However, when the problem size grows large in the lateral direction, the along-dip and along-strike Hausdorff measure can reach similar values. The results also indicate that for nonstratified deposits and horizontally stratified deposits, the Hausdorff measure obtained from horizontal and vertical data will be representative of the Hausdorff measure along dip and strike, respectively. For stratified and inclined deposits, the horizontal Hausdorff measure will not be representative of the along-dip Hausdorff measure, but the vertical Hausdorff measure can still be representative of the along-strike Hausdorff measure.

5. Discussion

5.1. Stationary RF

[25] Analysis of a synthetic ln(K) map based on an experimental stratigraphy offers insights into the spatial structure of sedimentary deposit. For selected regions of the map, experimental ln(K) variograms were first constructed along the major/minor statistical axes. The fitting of an exponential model onto the variograms is a model choice; a common practice in subsurface hydrology. Whether it is a good choice depends on whether the experimental variogram has a well-defined correlation structure, i.e., whether variogram levels off at a constant sill. Though the exponential model seems adequate for some stratified deposits (e.g., major variograms of the fluvial/floodplain deposits), other variograms increase systematically as the lag distance increases. For example, the minor variograms of the fluvial/floodplain deposits contain multiple structures with increasing variability levels (Figure 4; sample 9 and 10). This is due to the mixing of two facies types in the direction perpendicular to bedding: data pairs of contrasting ln(K) are used in constructing the minor variograms. The first structure at shorter lags has an integral scale of just a few Δz, which is on the same order of magnitude as the average thickness of the sand-rich and clay-rich units. *Lu and Zhang* [2002] and *Ritzi* [2000] have indeed found that the correlation range of stratified deposit corresponds to the harmonic mean of the thickness of all unit types. The upstream, sand-rich fluvial deposits (samples 2 and 3) have variograms that are not exponential. On the basis of transition probabilities, *Ritzi et al.* [2004] noted that "a sufficient condition for an exponential-like semivariogram is the repeated occurrence of unit types having both a contrast in permeability and a large length variance". These fluvial samples are fairly homogenous and characterized by a lack of distinct stratification. Because of the presence of faults, the major variogram of sample 3 also dips periodically as data pairs separated by these distances become more similar. The lag distances at these "dips" may thus characterize average fault spacing: the shortest lag corresponds to the average distance between two adjacent faults; larger lags to nonadjacent faults. In addition, the fluvial/floodplain deposit created in the upstream region of the basin (sample 11) is also faulted. The correlation structure for this sample is more complex: The ln(K) variogram map is a crisscrossing surface with two sets of correlation ellipses intersecting one another (Figure 7). One correlation structure set is parallel to the average bedding plane while the second set reflects fault orientation. The profile of the variogram map along the direction of the bedding plane is exponential, e.g., a correlation range may be determined by the average fault block width. The profile along faults has not reached a sill since most of the faults are truncated by the sample ($\lambda_{fault} > L_z$). Overall, multilevel correlation structure occurs due to statistical mixing at a given problem scale. This includes (1) minor variograms of stratified deposits where data pairs come from both sandy and clayey facies, (2) horizontal variograms of stratified deposits when the bedding plane is subhorizontal, and (3) nonstratified deposits intersected by high-conductivity faults.

[26] Correlation structure of a variogram is dependent on sample size compared to the size of the local heterogeneity. Compared to sample 9 and 10, the multilevel correlation structure becomes much more subdued in the minor variogram of sample 8 which has an overall linear shape for all lag distances. As the problem size grows to incorporate more data of similar statistics, the correlation structure may evolve, e.g., if sample 8 is increased to encompass the entire depositional environment, a larger-scale correlation structure may emerge as its minor variogram levels off at a higher sill, since the ln(K) variance within the fluvial/floodplain environment is finite (Figure 3c). This larger-scale variogram may thus describe the correlation not of an average sand/clay unit, but of the depositional environment which contains it. To test this hypothesis, a larger-scale exponential model is also fit to the minor variogram of sample 8, 9 and 10 (see the dashed line in Figure 4). An effective hydraulic conductivity ($\mathbf{K}^*$) is computed for each sample using a numerical flow approach [*Durlofsky*, 1991] and its principal components (K^*_{max}, K^*_{min}) estimated with an analytical model [*Gelhar and Axness*, 1983]. The analytical model utilizes the ln(K) variance and the statistical anisotropy ratio while assuming that (1) ln(K) is normally distributed; (2) its variogram structure is exponential. For each sample, the numerical flow approach computes an exact $\mathbf{K}^*$. When the larger-scale model is fit to the minor variograms, the analytical components of $\mathbf{K}^*$ improve in accuracy, especially for K^*_{min} (Table 3). This exercise strongly suggests that the depositional environment in this case constitutes a higher sedimentary hierarchy for which a global variogram (possibly stationary) exists with larger-scale range and sill. Therefore the concept of statistical mixing observed at one problem scale is relative. On the other hand, can we

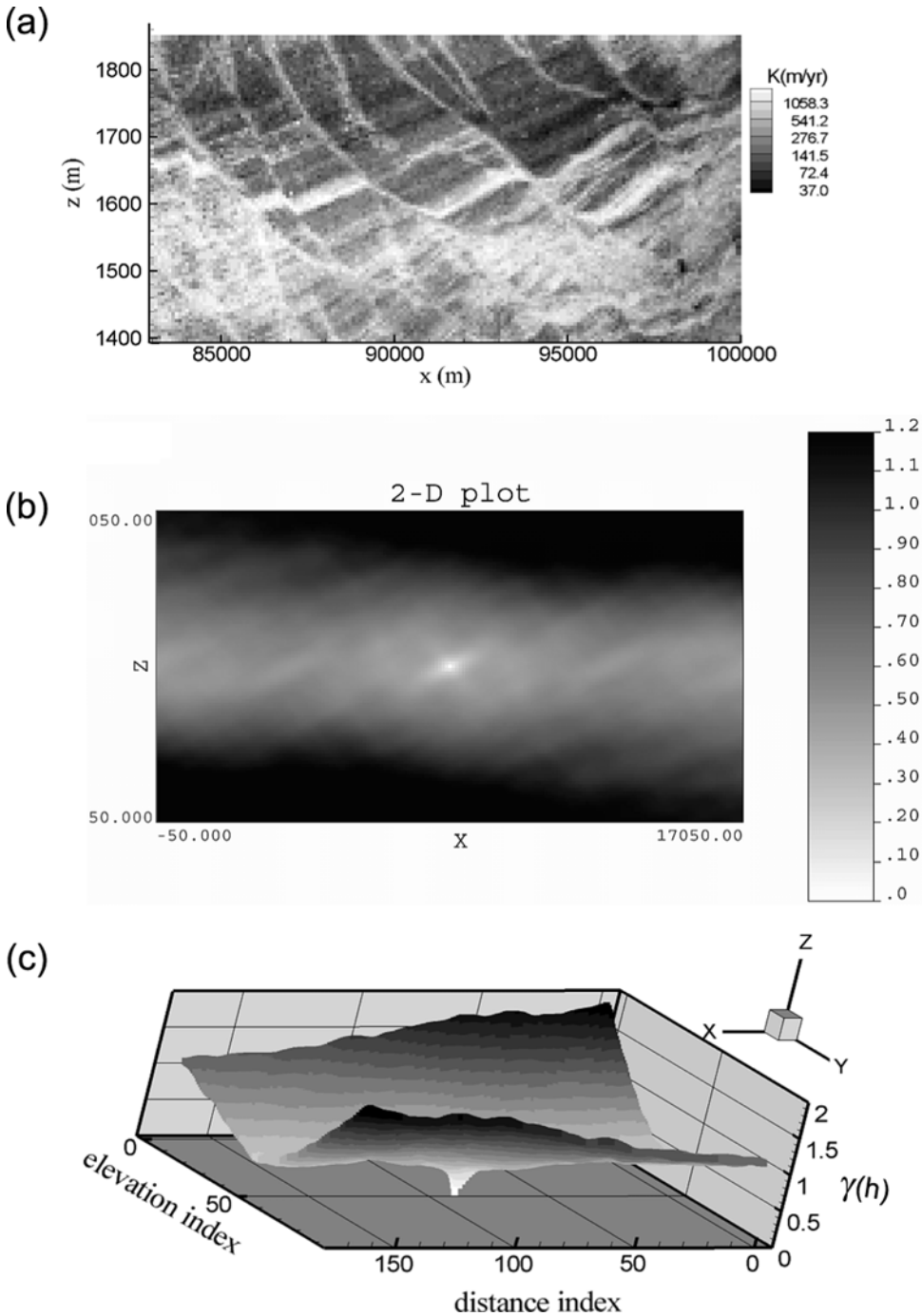

Figure 7. (a) The conductivity map of sample 11 (also shown in Figure 3a). (b) Plane view of the variogram map computed by GSLIB *varmap* [*Deutsch and Journel*, 1992]. (c) A surface view of Figure 7b. Note that the center of near zero variogram corresponds to zero lag distance.

expect to find a stationary variogram at a smaller scale? The answer is likely yes. The clue lies with the minor variograms of the turbidite deposits (samples 6 and 7) which display exponential structure with some "hole" effect. The stratified patterns of the turbidite deposits are similar to those of the fluvial/floodplain deposits, except only a few units are included. This indicates that if the fluvial/floodplain samples decrease in size, an exponential or "hole" effect behavior may arise, corresponding to the first level off in the multilevel variograms. Such behavior is not as obvious in the major variograms due to longer correlation length along the major axis compared to the lateral sample size ($\lambda_{max} \sim L_x$). However, some indication of the existence of a secondary structure may be seen in sample 8 as its major variogram rises above the exponential model at lag distance greater than 10 km. Although the search bandwidth for the major variograms limits data mixing across units, data pairs separated by a distance of 10 km and longer may constitute a larger-scale variability. In comparison, the smaller samples 9 and 10 have exponential-type major variograms. Therefore, depending on the average unit length/thickness relative to problem size L_x/L_z, the correlation structure may be exponential, "hole"

Table 3. Effective Hydraulic Conductivity Tensor **K*** of the Fluvial/Floodplain Deposits (Samples 8, 9, and 10) Computed With a Numerical Flow Approach[a]

							Small-Scale Minor Model						Large-Scale Minor Model					
			Numerical Flow (PBC), m/yr						*Gelhar and Axness* [1983]		Error, %				*Gelhar and Axness* [1983]		Error, %	
Sample	s_f^2	λ_{max}	**K***		K^*_{max}	K^*_{min}	λ_{min}	$\lambda_{max}/\lambda_{min}$	K^*_{max}	K^*_{min}	K^*_{max}	K^*_{min}	λ_{min}	$\lambda_{max}/\lambda_{min}$	K^*_{max}	K^*_{min}	K^*_{max}	K^*_{min}
8	0.38	1500	130.81 0.24	0.25 93.04	130.81	93.04	5	300	136.4	67.5	4.1	−37.9	500	3	127.4	98.1	−2.7	5.1
9	0.30	1500	114.10 0.07	0.08 90.58	114.10	90.58	10	150	117.9	56.5	3.2	−60.4	500	3	111.8	86.4	−2.1	−4.9
10	0.35	3500	19.46 0.05	0.05 15.10	19.46	15.10	7	500	20.1	10.1	3.4	−49.6	650	5.4	19.3	12.8	−0.6	−17.5

[a]The principal components of **K*** (m/yr) estimated with a stochastic-analytical model are also listed assuming a stationary ln(K) variogram.

effect, multilevel, or linear, until a larger-scale structure may appear.

[27] In a sedimentary deposit, the nonstationary correlation structure may be transitional between a stationary variogram representing a lower sedimentary hierarchy and one representing a higher hierarchy. Thus, upon careful selection of appropriate sample size, stationary variograms may occur in separate and discrete scales corresponding to distinct hierarchies. The stationarity assumption may be true only in a local sense and the conductivity spatial structure is continuously evolving as the problem scale changes. To illustrate this, we present a hypothetical sedimentary basin with five scales of heterogeneity (adapted from *Ahmadi and Quintard* [1996]): cross strata, cross-strata coset, facies, facies assemblage, and geologic formation (Figure 8). At a particular hierarchy, ln(K) variogram may exhibit different correlation structure depending on the size of the local geological structure compared to problem size. The variogram shape alone thus may not be indicative of the type of the underlying deposit. Instead, parameters such as the range, the sill and the knowledge of the size, shape and variability of the local sedimentary structure are needed. Within a hierarchical system, if models are fit onto the local variograms, the correlation range estimated would become dependent on the problem size and its interpretation depend on the largest geological feature the problem contains [*Gelhar*, 1993]. For example, it may range from less than a meter to meter-scale representing the correlation of deposits at the scale of the cross strata, to tens or hundreds of meters representing the correlation of deposits at facies to facies assemblage scale, to greater than km for an entire geological formation. Porosity well logs measured in a fluvial deposit [*Barrash and Clemo*, 2002] provide further evidence to support this view. In this study, vertical porosity variograms were computed for different sedimentary hierarchies and are characterized by stationary variograms of increasing range and sill as the sample domain incorporates ever larger scales of the deposits. Therefore, to establish a study area where it is ideal to have stationary correlation structure (common assumption for stochastic flow and transport models), a problem size has to be carefully chosen for a given geological medium. If ln(K) is locally characterized by normality and stationary correlation structure, stochastic-analytical model prediction on the effective hydraulic conductivity will become more accurate. On the other hand, variogram model fitting onto experimental variograms should consider the possible emergence of larger-scale correlation structures. If a parameter set shows no visible trends, it is questionable to detrend a variogram with apparent nonstationary features. To help identify an appropriate problem size, information based on the regional facies map or geological insights on the extent of deposition can be helpful. In a cross-sectional study, information about the bedding angle would also be useful to help identify the statistical axis of correlation. In this study, a large-scale stationarity may be assumed for the depositional environment, and a smaller stationarity may be assumed at the facies scale. In a basin scale problem, zonation based on facies types may be extended to a higher hierarchy depending on the depositional environment type (basis for the geological framework models).

[28] In light of the above discussions, the two-level experimental variograms observed at the Cape Cod site could be explained by two disparate scales of local stationarity: the small problem size (20 m × 7 m) from the flowmeter measurements may represent a lower sedimentary hierarchy while the larger problem size (5 km × 50 m) from the slug test measurements may represent a higher variability (Figure 9). The sill of the flowmeter variogram is approaching the nugget of the slug test variogram, consistent with known causes of "nugget effect", that is, besides measurement errors, the small-scale variability not captured by the sampling grid can contribute to a nugget effect in the larger-scale variogram. Under the hierarchical assumption of local stationarity, two exponential models are fit: one onto the small-scale flowmeter data variogram and one onto the large-scale slug test data variogram. Each model gives a correlation range that is representative of the spatial continuity specific to a hierarchy. A geological interpretation for the increasing correlation range may thus be offered. For the small problem size, the correlation range may represent the average length of high-conductivity lenses. For the large problem size, it may represent the average length of geological facies which contain these lenses.

5.2. Stochastic Fractal

[29] Self-affine stochastic fractal is a useful empirical tool in modeling a variety of geological phenomena, e.g., downhole geophysical parameters of crystalline basement rocks were found to be fractal scaling with a spectral slope within the range of [0.5, 1.5] [*Leonardi and Kumpel*, 1998]. The

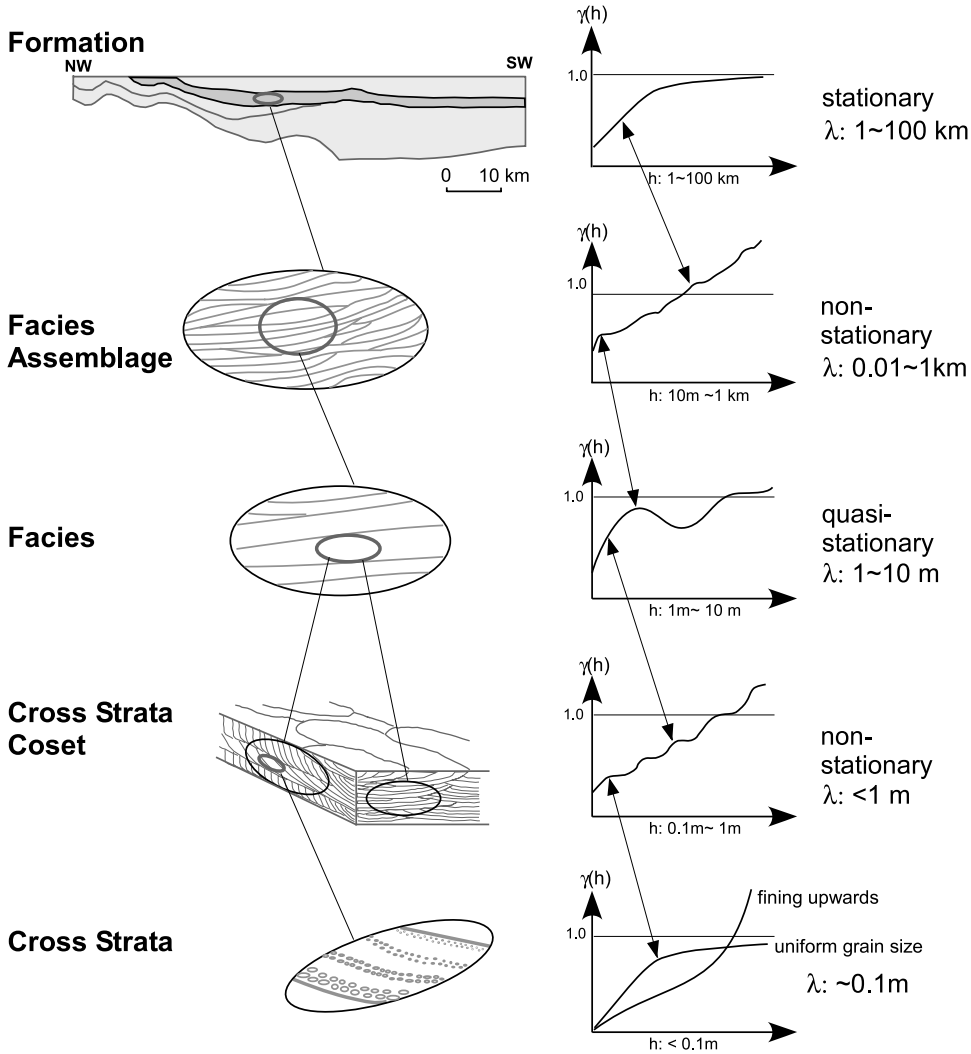

Figure 8. A schematic diagram showing the variogram structure as the scale of the problem increases in a hypothetical basin with five scales of sedimentary hierarchy. The sample domain is indicated with the black outline. The thick gray circle indicates a subscale. The experimental (minor) variograms are normalized by the sample variance. Here λ is the correlation scale.

log permeability of clastic coarse-grained reservoir rocks from north central North Sea Brae oil well cores has a spectral slope within the range of [0.6, 1.4] [*Leary and Al-Kindy*, 2002]. Analysis of vertical porosity well log from a deep submarine sandstone formation yielded a spectral slope of 0.71 [*Hewett*, 1986], while vertical density log from a carbonate reservoir yielded a spectral slope of 0.78 [*Tubman and Crane*, 1995]. Porosity logs from 15 wells drilled in a deltaic environment in the Gulf of Mexico give a spectral slope of 1.4 with a standard deviation of 0.2 [*Pelletier and Turcotte*, 1996]. However, within the same basin, vertical geophysical well logs of a multifacies sand/shale deposit from a fluvial/deltaic system give a spectral slope ranging from 1.4 to 2.1 [*Deshpande et al.*, 1997], higher than the other data and falling outside the range of $1/f$ noise.

[30] In this study, to directly compare the range of the spectral slope obtained from the vertical variogram analysis of the selected samples with those obtained from natural deposits, a conceptual normalized spectral density is presented, superimposed with the ranges of spectral slope found for both natural deposits and the experimental deposit (Figure 10). We also computed the power spectrum for 11 vertical synthetic boreholes evenly spaced across our ln(K) map; a spectral slope for each borehole is obtained by direct power law model fitting with equation (4). All boreholes transect the entire thickness of the basin, crossing multiple depositional environments. The spectral slope of the synthetic boreholes has a range of 1.38 to 2.25, closely matching that found for the sand/shale system [*Deshpande et al.*, 1997]. Moreover, from Figure 10, we notice that the range of the spectral slope (β) seems to increase from the possibly single-"facies" data of *Hewett* [1986] and *Tubman and Crane* [1995] to our vertical synthetic well bores and the data from the sand/shale system [*Deshpande et al.*, 1997] which are characterized with multiple facies and/or depositional environments. The spectral slope obtained from the vertical variograms of the 13 samples (each representing deposit of a single depositional environment containing 1 or 2 facies types) falls in between these two groups. Thus it appears that the magnitude of the vertical spectral slope may depend on the number of facies that are

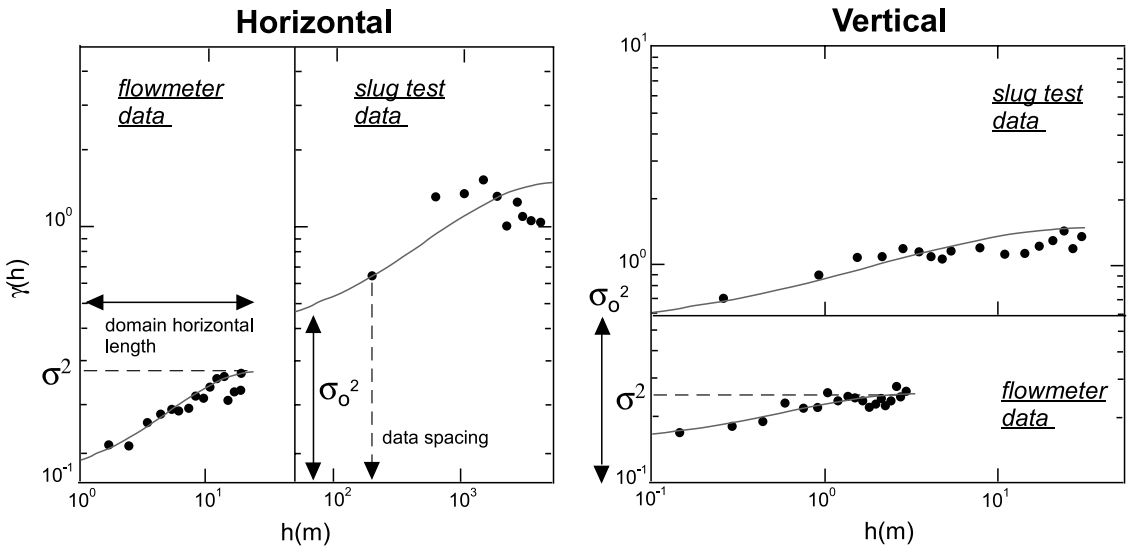

Figure 9. Cape Cod experimental variograms (dots) reinterpreted. An exponential model (curve) is fit onto each hierarchical variogram. Here σ^2 is the sill of the small sample from the flowmeter measurements; σ_o^2 is the nugget of the large sample from the slug test measurements.

incorporated for a given problem. If only one facies is incorporated, the magnitude of the spectral slope will be low, reflecting the dominance of short-range variability within the facies; if two or more facies is incorporated for a given problem, the spectral slope may become higher, reflecting the gradual dominance of the long-range variability among multiple facies. That is, if different facies units are repeating in the vertical direction, the large-scale be-

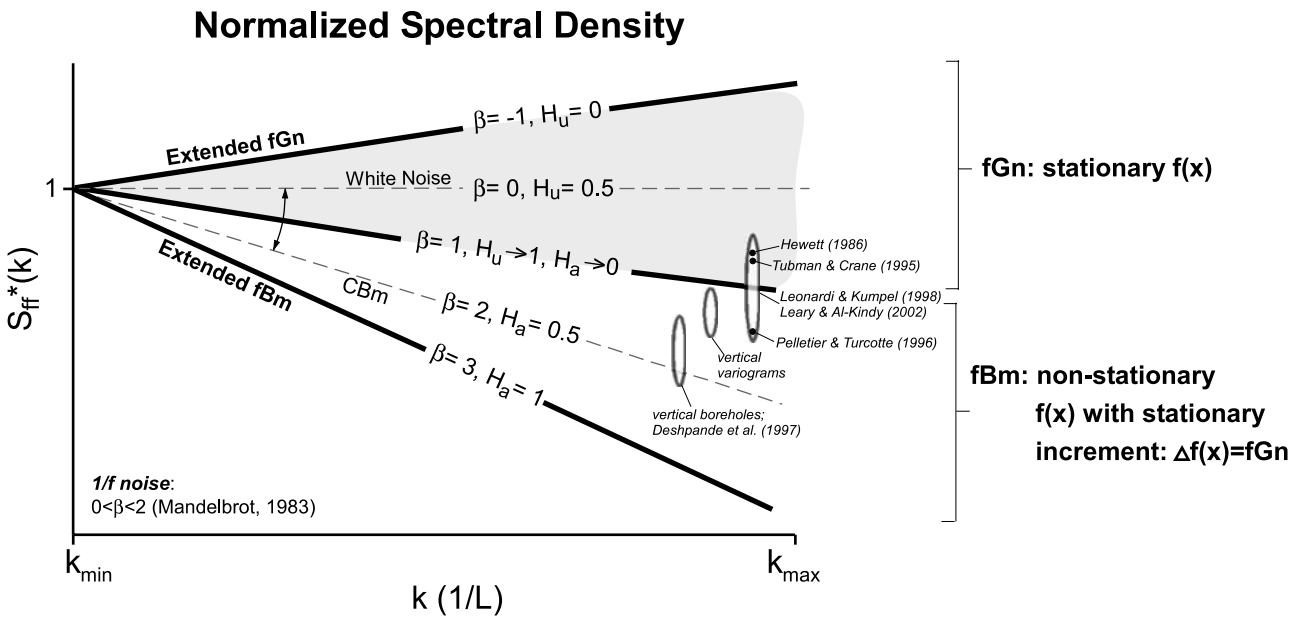

Figure 10. Schematic diagram of a normalized spectral density for fGn and fBm of a 1-D stochastic fractal f(x). Both axes are in log unit. $S_{ff}^*(k)$ is the normalized spectral density: $S(k)/S(k_{min})$. For a stochastic fractal, $S(k) = |F(k)|^2 \sim k^{-\beta}$ ($-1 < \beta < 1$: fGn; $1 < \beta < 3$: fBm), F(k) is the Fourier transform of f(x) in the wave number space. Note that fBm increment is fGn for which the spectral slope is usually related to a Hurst coefficient ($\beta = 2H_u - 1$; $0 < H_u < 1$); for fBm, the spectral slope is usually related to a Hausdorff measure ($\beta = 2H_a + 1$; $0 < H_a < 1$) [*Turcotte*, 1997]. Note that $\beta = 0$ is the white noise (flat spectrum when $f(x) = \delta(x)$, $\delta(x)$ is the Dirac delta-function); $\beta = 2$ is the classical Brownian motion (CBm) for which the increment process is white noise. Note also that when $-1 < \beta < 0$, f(x) is a negatively correlated fGn; when $0 < \beta < 1$, f(x) is positively correlated fGn; when $1 < \beta < 2$, f(x) is fBm whose increment is the negatively correlated fGn (antipersistence); when $2 < \beta < 3$, f(x) is fBm whose increment is the positively correlated fGn (persistence). Thus, if the series is modeled as a fBm, its increment series is fGn with $\beta_{inc} = \beta - 2$.

tween-facies variability will dominate over the small-scale within-facies variability. A similar observation is noted for a synthetic and stratified deposits by *Ritzi et al.* [2004], who found that the transition probability of different facies units is responsible for most of the ln(K) variance or variogram shape. Thus, depending on the problem size and whether multiple facies are incorporated for the problem, permeability, porosity or other geophysical properties have indeed been modeled sometimes as fGn, sometimes as fBm, e.g., data collected from a single facies have lower spectral slope, thus fGn is considered appropriate. This is also the source of considerable confusion in the literature as sometimes a Hurst coefficient is estimated (if fGn is assumed as the appropriate model), and sometimes a Hausdorff measure is estimated (if fBm is assumed as the appropriate model) [*Painter*, 2003]. In this study, we followed the terminology presented by *Turcotte* [1997] and used the spectral slope to distinguish between the different stochastic series. In addition, the along-dip Hausdorff measure estimated for different deposits increases from the relatively homogenous deepwater and fluvial deposits to the stratified deposits formed by fluvial/floodplain and deltaic processes, due to the fact that the laterally extensive and stratified deposits have more spectral energy distributed over the lower wave number space (long-range variability), vice versa. Therefore the fractal ''signature'' of the sedimentary deposits is not only problem scale-dependent, but also depositional processes-dependent. Finally, although the stationary assumption of a RF seems at odds with the self-affine assumption, in a hierarchical system, the overall pattern in variogram structure may emerge in a scale-invariant fashion: different variogram structures (be it stationary or nonstationary) reoccur as the sample domain incorporates ever larger scales of the sedimentary hierarchy (Figure 8). This mirrors the statistical self-affinity predicted by the power law model.

6. Conclusions

[31] The synthetic ln(K) map based on the experimental stratigraphy provides us with a rich data set to explore various long-standing problems associated with heterogeneous deposits. For example, the scale dependency of the univariate and bivariate statistics, the directional sensitivity of the Hausdorff measure, the applicability of the analytic-stochastic theories to infer the effective properties, the relationship between the ''scale effects'' of the effective properties and the underlying sedimentary heterogeneity, and solute transport in nonstationary media. Besides assigning to each pixel a conductivity value and an associated REV size, the conductivity map does not involve other assumptions often associated with synthetic data sets. For example, a stratigraphic model by *Scheibe and Freyberg* [1995] was created by assuming uniform within-unit permeability and large-scale continuity of sedimentary structures. In our map, there is no abrupt cutoff at any scale of the deposit beneath which heterogeneity no longer exists. Within many stratified deposits, there also exists long-range correlation exhibited as continuous sedimentary layers or faults that can transect much of the length scale of a depositional environment. The requirement of the classic stochastic theories that a problem size has to be many times the correlation range is not satisfied in many parts of our basin.

[32] In this work, we present the results of a geostatistical analysis which represent the initial effort of our overall goal of understanding the above issues. We found that in a hierarchical sedimentary system, the shape of the experimental variogram depends on the sample domain size in relation to the size of the local-scale heterogeneity. Stationary correlation structure may occur at separate and distinct scales each corresponding to a particular hierarchy; the fitted correlation range thus becomes dependent on the problem size. For a given problem, multilevel correlation structure can occur due to statistical mixing, i.e., data pairs come from different facies types. The two-level variograms of the Cape Cod site may be explained by two disparate scales of local stationarity. On the other hand, assuming ln(K) is a stochastic fractal, the Hausdorff measure obtained has a comparable range to natural geological deposits. It tends to increase from nonstratified to stratified deposits with a cutoff value at 0.15, and, it also increases as the number of facies incorporated in a problem increases. This implies that fractal characteristic of sedimentary rocks is both process-dependent and problem-scale-dependent.

[33] Future analysis can include the evaluation of the link between indicator statistics and variograms based on the continuous variable. By assuming conductivity cutoffs, indicator variograms and transition probabilities can be computed. Along with the local within-facies property distribution, a hierarchical variogram analysis may be conducted [*Ritzi et al.*, 2004]. In such an analysis, data sampling will come from several depositional environments, incorporating more than two facies. Effective hydrological properties can be evaluated for the heterogeneous deposits. The link between the statistical measures of ln(K) (mean, variance, variogram correlation, Hausdorff measure), the ''scale effect'' in the effective hydraulic conductivity and macrodispersivity, and the existence of a regional-scale REV for each depositional environment can be explored. Different geological framework models can be constructed and flow and transport modeling in both the fully heterogeneous model and the framework models can be conducted. The impact of effective parameterization on a variety of geological processes can be assessed, e.g., salt water intrusion, ore formation, past climate reconstruction, reactive transport, oil/gas migration, waste isolation via deep well injection, and more. In addition, different geostatistical interpolation and simulation methods can be evaluated given a subset of the data. The effect of the change of support is also of interest since statistics often change as the data support changes. Finally, for both the prototype experiment of 1996 and the larger-scale 1999 experiment, three-dimensional stratigraphies have been created based on digital reconstructions of the two-dimensional dissections. To analyze the correlation structure in three dimensions, multiple point statistics may be needed to better describe the conductivity variation in deposits where curvilinear features dominate. Groundwater flow, heat transfer and solute transport in the fully heterogeneous three-dimensional systems will be of significant interest.

[34] In using the experimental stratigraphy to study the heterogeneity-related issues, we must emphasize that the

experimental deposit should not be viewed as an exact analog for natural sedimentary rocks. The experimental deposit must be viewed as nothing more or less than a set of strata, fully accessible in three dimensions, produced under controlled conditions by processes that represent a subset of those active in natural systems. These include important forms of self-organization and spontaneous pattern formation that are common in nature yet difficult to capture in simulation models. However, due to the intrinsic constraints of the experiment (e.g., using coal to represent clay; geometry of the experimental setting produces a more exaggerated topographic slope, lack of representation of biogenic processes and Coriolis effect), and the assumptions employed to create the synthetic ln(K) map, caution must be exerted in any effort to directly compare our results with those found in natural sedimentary systems the experiment attempts to emulate. It is important to point out that in a natural fluvial/deltaic system, stratification can occur at more scales, e.g., cross strata can result from bed load versus suspended load transport, layers of point bar deposits can result from lateral migration of channels, periodic flooding can result in alternations of channel (sandy) and floodplain (clayey) facies, and sea level variation or tectonic subsidence can result in change in depositional environment from fluvial sand/clay system to marine deepwater clay, thus creating the largest scale stratification. In the prototype experiment from which our data came, the finer scales of stratifications (cross strata or point bar deposits) were not created due to the lack of truly channellized flows. However, future experiments are continuously being designed to create more realistic fluvial processes and accordingly, finer scales of stratifications. For example, in the 1999 experiment, more channellized systems were developed within a larger accommodation space from which we can observe the formation of point bars. Since multiscale stratification is most likely responsible for the fractal signature of the various geophysical properties of sedimentary rocks, any ''physical theory'' developed should explain the stratification observed at all scales as a result of a variety of sediment transport mechanisms. Over time, we hope that the experiments will help us obtain better understanding of the underlying physical processes as well as better characterization of the multiscale, hierarchical sedimentary heterogeneity.

[35] **Acknowledgments.** We wish to thank Andre Journel from Stanford University, Fred Molz from Clemson University, Efi Foufoula from the University of Minnesota, Lu Silong from Tetra Tech, Inc., W. Pelletier from the University of Arizona, and two anonymous reviewers for their valuable insights and suggestions. The work was supported by Institute of Geophysics and Planetary Physics, Los Alamos National Laboratory.

References

Ahmadi, A., and M. Quintard (1996), Large-scale properties for two-phase flow in random porous media, in *Effective Parameter Estimation for Flow and Transport in the Subsurface*, edited by. J. J. Gomez-Hernandez, Elsevier, New York.

Barrash, W., and T. Clemo (2002), Hierarchical geostatistics and multifacies systems: Boise Hydrogeophysical Research Site, Boise, Idaho, *Water Resour. Res.*, *38*(10), 1196, doi:10.1029/2002WR001436.

Bear, J. (1972), *Dynamics of Fluids in Porous Media*, 764 pp., Dover, Mineola, N. Y.

Belitz, K., and J. D. Bredehoeft (1990), Role of confining layers in controlling large-scale regional groundwater flow, in *Hydrogeology of Low Permeability Environment*, edited by S. P. Neuman and I. Neretnieks, pp. 7–17, Verlag H.Heise, Hannover, Germany.

Caers, J., and T. Zhang (2004), Multiple-point geostatistics: a quantitative vehicle for integrating geologic analogs into multiple reservoir models, in *Integration of Outcrop and Modern Analogs in Reservoir Modeling*, *AAPG Mem.*, *80*, 1–24.

Chilès, J.-P., and P. Delfiner (1999), *Geostatistics: Modeling Spatial Uncertainty*, 695 pp., Wiley-Interscience, Hoboken, N. J.

Desbarats, A. J., and S. Bachu (1994), Geostatistical analysis of aquifer heterogeneity from the core scale to the basin scale: A case study, *Water Resour. Res.*, *30*, 673–684.

Deshpande, A., P. B. Flemings, and J. Huang (1997), Quantifying lateral heterogeneities in fluvio-deltaic sediments using three-dimensional reflection seismic data: Offshore Gulf of Mexico, *J. Geophys. Res.*, *102*(B7), 15,385–15,401.

Deutsch, C. V. (2002), *Geostatistical Reservoir Modeling*, Oxford Univ. Press, New York.

Deutsch, C. V., and A. G. Journel (1992), *GSLIB: Geostatistical Software Library and User's Guide*, 340 pp., Oxford Univ. Press, New York.

Durlofsky, L. J. (1991), Numerical calculation of equivalent grid block permeability tensors for heterogeneous porous media, *Water Resour. Res.*, *27*, 699–708.

Englund, E., and A. Sparks (1988), Geo-Eas user's guide: Geostatistical environmental assessment software, *Rep. EPA/600/4-88/033a*, 130 pp., U.S. Environ. Prot. Agency, Washington, D. C.

Federico, V. D., and S. P. Neuman (1997), Scaling of random fields by means of truncated power variograms and associated spectra, *Water Resour. Res.*, *33*, 1075–1085.

Freeze, R. A., and J. A. Cherry (1979), *Groundwater*, 604 pp., Prentice-Hall, Upper Saddle River, N. J.

Gelhar, L. W. (1993), *Stochastic Subsurface Hydrology*, Prentice-Hall, Upper Saddle River, N. J.

Gelhar, L. W., and C. L. Axness (1983), Three-dimensional stochastic analysis of macrodispersion in aquifers, *Water Resour. Res.*, *19*, 161–180.

Heller, P. L., C. Paola, I. G. Hwang, B. John, and R. Steel (2001), Geomorphology and sequence stratigraphy due to slow and rapid base-level changes in an experimental subsiding basin (XES 96-1), *AAPG Bull.*, *85*(5), 817–838.

Hewett, T. A. (1986), Fractal distribution of reservoir heterogeneity and their influence on fluid transport, paper SPE 15,386 presented at 61st Annual Society of Petroleum Engineers Technical Conference, Soc. of Pet. Eng., New Orleans, La.

Koltermann, C., and S. M. Gorelick (1995), The fractional packing model for hydraulic conductivity derived from sediment mixtures, *Water Resour. Res.*, *31*, 3283–3297.

Leary, P. C., and F. Al-Kindy (2002), Power-law scaling of spatially correlated porosity and log (permeability) sequences form north-central North Sea Brae oilfield well core, *Geophys. J. Int.*, *148*, 426–442.

Leonardi, S., and H.-J. Kumpel (1998), Variability of geophysical log data and the signature of crustal heterogeneities at KTB, *Geophys. J. Int.*, *135*(3), 964–974.

Liu, H. H., and F. J. Molz (1996), Discrimination of fractional Brownian movement and fractional Gaussian noise structures in permeability and related property distributions with range analyses, *Water Resour. Res.*, *32*, 2601–2605.

Liu, H. H., and F. J. Molz (1997), Fractional Brownian motion and fractional Gaussian noise in subsurface hydrology: A review, presentation of fundamental properties, and extensions, *Water Resour. Res.*, *33*, 2273–2286.

Lu, S., F. J. Molz, G. E. Fogg, and J. W. Castle (2002), Combining stochastic facies and fractal models for representing natural heterogeneity, *Hydrogeol. J.*, *10*, 475–482.

Lu, Z., and D. Zhang (2002), On stochastic modeling of flow in multimodal heterogeneous formations, *Water Resour. Res.*, *38*(10), 1190, doi:10.1029/2001WR001026.

Mandelbrot, B. B. (1983), *The Fractal Geometry of Nature*, W. H. Freeman, New York.

Molz, F. J., and G. K. Boman (1993), A fractal-based stochastic interpolation scheme in subsurface hydrology, *Water Resour. Res.*, *29*, 3769–3774.

Molz, F. J., and G. K. Boman (1995), Further evidence of fractal structure in hydraulic conductivity distributions, *Geophys. Res. Lett.*, *22*, 2545–2548.

Molz, F. J., H. Rajaram, and S. Lu (2004), Stochastic fractal-based models of heterogeneity in subsurface hydrology: Origins, applications, limita-

tions, and future research questions, *Rev. Geophys.*, *42*, RG1002, doi:10.1029/2003RG000126.

Neuman, S. P. (1990), Universal scaling of hydraulic conductivities and dispersivities in geologic media, *Water Resour. Res.*, *26*, 1749–1758.

Neuman, S. P. (1994), Generalized scaling of permeabilities: Validation and effect of support scale, *Geophys. Res. Lett.*, *21*, 349–352.

Painter, S. (2003), Statistical characterization of spatial variability in sedimentary rock, in *Heterogeneity in the Crust and Upper Mantle: Nature, Scaling and Seismic Properties*, edited by J. A. Goff and K. Holliger, pp. 187–206, Springer, New York.

Painter, S., and L. Paterson (1994), Fractional Levy motion as a model for spatial variability in sedimentary rock, *Geophys. Res. Lett.*, *21*, 2857–2860.

Paola, C. (2000), Quantitative models of sedimentary basin filling, *Sedimentology,*, *47* suppl. 1, 121–178.

Paola, C., et al. (2001), Experimental stratigraphy, *GSA Today*, *11*(7), 4–9.

Pelletier, J. D., and D. L. Turcotte (1996), Scale-invariant topography and porosity variations in fluvial sedimentary basins, *J. Geophys. Res.*, *101*(B12), 28,165–28,175.

Pratson, L., and W. Gouveia (2002), Seismic simulations of experimental strata, *AAPG Bull.*, *86*(1), 129–144.

Rajaram, H., and L. W. Gelhar (1995), Plume-scale dependent dispersion in aquifers with a wide range of scales of heterogeneity, *Water Resour. Res.*, *31*, 2469–2482.

Rehfeldt, K. R., J. M. Boggs, and L. W. Gelhar (1992), Field study of dispersion in a heterogeneous aquifer: 3. Geostatistical analysis of hydraulic conductivity, *Water Resour. Res.*, *28*, 3309–3324.

Ritzi, R. W. (2000), Behavior of indicator semivariograms and transition probabilities in relation to the variance in lengths of hydrofacies, *Water. Resour. Res.*, *36*(11), 3375–3381.

Ritzi, R. W., Z. Dai, D. F. Dominic, and Y. N. Rubin (2004), Spatial correlation of permeability in cross-stratified sediment with hierarchical architecture, *Water Resour. Res.*, *40*, W03513, doi:10.1029/2003WR002420.

Scheibe, T. D., and D. L. Freyberg (1995), Use of sedimentological information for geometric simulation of natural porous media structure, *Water Resour. Res.*, *31*, 3259–3270.

Schneider, D. (1998), Tectonics in a sand box, *Sci. Am.*, *279*, 36.

Springer, R. A. (1991), Application of an improved slug-test analysis to the large-scale characterization of heterogeneity in a Cape Cod aquifer, M. S. thesis, Mass. Inst. of Technol., Cambridge.

Sudicky, E. A. (1986), A natural gradient experiment on solute transport in a sand aquifer: Spatial variability of hydraulic conductivity and its role in the dispersion process, *Water Resour. Res.*, *22*, 2069–2082.

Tidwell, V. C., and J. L. Wilson (2002), Visual attributes of a rock and their relationship to permeability: A comparison of digital image and minipermeameter data, *Water Resour. Res.*, *38*(11), 1261, doi:10.1029/2001WR000932.

Tubman, K. M., and S. D. Crane (1995), Vertical versus horizontal well log variability and application to fractal reservoir modeling, in *Fractals in Petroleum Geology and Earth Processes*, edited by C. C. Barton and P. R. La Pointe, pp. 279–293, Elsevier, New York.

Turcotte, D. L. (1997), *Fractals and Chaos in Geology and Geophysics*, 398 pp., Cambridge Univ. Press, New York.

J. M. Davis, Department of Earth Sciences, University of New Hampshire, 56 College Road, Durham, NH 03824, USA.

C. W. Gable, EES-6, MS T003, Los Alamos National Laboratory, Los Alamos, NM 87545, USA.

C. Paola, Department of Geology and Geophysics, University of Minnesota, 310 Pillsbury Drive SE, Minneapolis, MN 55455, USA.

M. Person, Department of Geological Sciences, Indiana University, 1001 East 10th Street, Bloomington, IN 47405, USA.

X.-H. Wen, Chevron Texaco, ETC, 6001 Bollinger Canyon Road, San Ramon, CA 94583, USA.

Y. Zhang, Department of Geological Sciences, University of Michigan, 2534 C. C. Little Building, 1100 North University Avenue, Ann Arbor, MI 48109, USA. (ylzhang@umich.edu)